HHS Public Access

Author manuscript

Cell Rep. Author manuscript; available in PMC 2024 September 20.

Published in final edited form as:

Cell Rep. 2024 July 23; 43(7): 114379. doi:10.1016/j.celrep.2024.114379.

The PP2A regulatory subunit PPP2R2A controls NAD+ biosynthesis to regulate T cell subset differentiation in systemic autoimmunity

Wenliang Pan[1,*], **Maria G. Tsokos**[1], **Marc Scherlinger**[1,2], **Wei Li**[1], **George C. Tsokos**[1,3,*]

[1]Department of Medicine, Beth Israel Deaconess Medical Center and Harvard Medical School, Boston, MA, USA

[2]Rheumatology Department, Strasbourg University Hospital of Hautepierre, Strasbourg, France

[3]Lead contact

SUMMARY

The protein phosphatase 2A (PP2A) regulatory subunit PPP2R2A is involved in the regulation of immune response. We report that lupus-prone mice with T cells deficient in PPP2R2A display less autoimmunity and nephritis. PPP2R2A deficiency promotes NAD^+ biosynthesis through the nicotinamide riboside (NR)-directed salvage pathway in T cells. NR inhibits murine Th17 and promotes Treg cell differentiation, *in vitro*, by PARylating histone H1.2 and causing its reduced occupancy in the *Foxp3* loci and increased occupancy in the *Il17a* loci, leading to increased *Foxp3* and decreased *Il17a* transcription. NR treatment suppresses disease in *MRL.lpr* mice and restores NAD^+-dependent poly [ADP-ribose] polymerase 1 (PARP1) activity in CD4 T cells from patients with systemic lupus erythematosus (SLE), while reducing interferon (IFN)-γ and interleukin (IL)-17 production. We conclude that PPP2R2A controls the level of NAD^+ through the NR-directed salvage pathway and promotes systemic autoimmunity. Translationally, NR suppresses lupus nephritis in mice and limits the production of proinflammatory cytokines by SLE T cells.

Graphical abstract

*Correspondence: wpan2@bidmc.harvard.edu (W.P.), gtsokos@bidmc.harvard.edu (G.C.T.).

AUTHOR CONTRIBUTIONS

W.P. designed and performed the experiments, analyzed the data, and wrote the manuscript. M.G.T. analyzed the data, provided critical expertise, and edited the manuscript. M.S. helped to perform the experiments with mice. W.L. performed the experiments involving human cells. G.C.T. conceived and supervised the study, interpreted the data, and wrote the manuscript.

SUPPLEMENTAL INFORMATION

Supplemental information can be found online at https://doi.org/10.1016/j.celrep.2024.114379.

DECLARATION OF INTERESTS

The authors declare no competing interests.

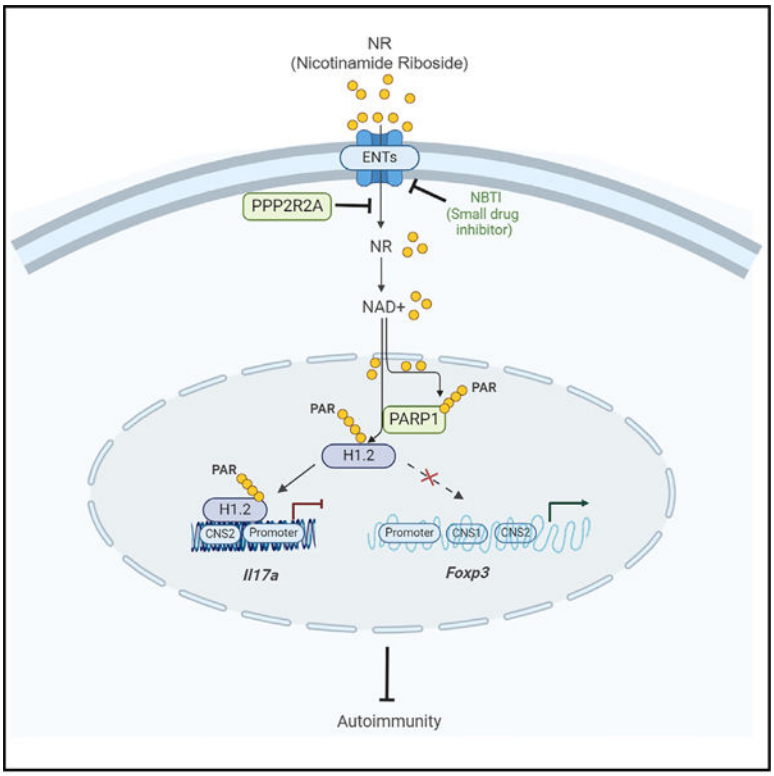

In brief

Pan et al. report that PPP2R2A deficiency in T cells promotes NAD^+ biosynthesis through the NR-directed salvage pathway and attenuates autoimmunity and nephritis in lupus-prone mice. NR inhibits Th17 and promotes Treg cell differentiation by PARylating histone H1.2. Translationally, NR suppresses lupus nephritis in mice and limits proinflammatory cytokine production by SLE T cells.

INTRODUCTION

The development of systemic autoimmunity and organ inflammation involves altered production of cytokines by T cells.[1–3] Specifically, decreased interleukin (IL-2) production accounts for decreased cytotoxic T cell function and decreased function and numbers of regulatory T (Treg) cells,[2] whereas the increased production of IL-17 and interferon (IFN)-γ may contribute directly to organ inflammation.[4]

T cell subset differentiation and function involves distinct metabolic reprogramming to support their unique energetic demands.[5] For example, T helper 1 (Th1) and Th17 cells utilize mainly aerobic glycolysis and glutaminolysis, while naive CD4 and Treg cells use primarily fatty acid oxidation and oxidative phosphorylation.[6] T cells from patients with systemic lupus erythematosus (SLE), the archetypic autoimmune disease, exhibit significant metabolic aberrations[7] which can alter gene expression by modulating the epigenetic landscape[8] and promote the differentiation of T cells toward a proinflammatory phenotype.[8] Although some of them may reflect chronic activation, others may be

genetically determined, as suggested by the association of SLE with risk alleles in genes that control mitochondrial ATP production (i.e., *MT-ATP6* and *UCP2*).[9,10] Inhibitors targeting the metabolic pathway have been used to treat mice with a lupus-like disease. For instance, the combination of metformin, an inhibitor of the mitochondrial electron transport chain complex I, and 2DG (2-deoxy-D-glucose), a glucose metabolism inhibitor, decreased autoimmunity and nephritis in lupus-prone mice.[11] Additionally, treatment with an inhibitor of mitochondrial F1F0 ATP synthase, 1,4-benzodiazepine (Bz-423), led to the apoptosis of autoreactive CD4 T cells and the suppression of glomerulonephritis[12], and pharmacologic inhibition of glutaminase 1, an enzyme that is in charge of converting glutamine to glutamate, reduced Th17 cell differentiation and disease activity in *MRL.lpr* mice.[13,14]

Protein phosphatase (PP) 2A is a ubiquitously expressed and highly conserved serine/threonine phosphatase that plays an essential role in multiple cellular processes, including cell division, cytoskeletal dynamics, and various signaling pathways.[15] The PP2A core enzyme consists of the scaffold subunit A ($PP2A_A$) and the catalytic subunit C ($PP2A_C$). To form a functional holoenzyme, the core enzyme interacts with one of the many regulatory subunits ($PP2A_B$) that define its function and tissue specificity.[16] It has been shown that the mRNA and protein levels as well as the catalytic activity of $PP2A_C$ are increased in T cells from patients with SLE,[17,18] and transgenic mice overexpressing $PP2A_C$ in T cells develop glomerulonephritis in an IL-17-dependent manner.[19] Furthermore, PP2Ac is requisite for Treg cell function by regulating mammalian target of rapamycin complex 1 activity.[20] PP2A regulatory subunits serve distinct T cell functions, with PPP2R2B being responsible for the IL-2 deprivation-induced T cell apoptosis,[21] PPP2R2D (PR55δ) for limiting IL-2 production and Treg cell function,[22] and PPP2R2A (PR55α) for promoting Th1 and Th17 differentiation.[23]

To further dissect the role of PPP2R2A in the development of lupus-like disease, we generated *B6.lpr.dLck^{Cre}R2A$^{fl/fl}$* mice, which lack PPP2R2A only in T cells. Mice with T cell-specific PPP2R2A deficiency developed less systemic autoimmunity and nephritis. Metabolomics data revealed that PPP2R2A deficiency promoted nicotinamide (NAM) adenine dinucleotide (NAD^+) production through the nicotinamide riboside (NR)-directed salvage biosynthesis pathway. Of translational value is our observation that NR supplementation significantly inhibited *in vitro* murine Th1 and Th17 differentiation, promoted Treg cell differentiation, and reduced significantly lupus-related pathology in *MRL.lpr* mice. Mechanistically, NR increased the levels of NAD^+ and caused PARylation of histone H1.2, leading to reduced occupancy in the *Foxp3* gene locus but increased occupancy in the *Il17a* gene locus, promoting *Foxp3* gene transcription, and decreasing *Il17a* gene transcription. Finally, the NAD^+-dependent poly [ADP-ribose] polymerase 1 (PARP1) enzymatic activity was found to be decreased in CD4 T cells from patients with SLE, and the addition of NR restored PARP1 activity and reduced IFN-γ and IL-17 expression in CD4 T cells from patients with SLE.

RESULTS

PPP2R2A deficiency in T cells alleviates disease in lupus-prone mice

We have reported that PPP2R2A is upregulated in T cells from patients with SLE, and that genetic PPP2R2A deficiency in murine T cells reduces Th1 and Th17 differentiation and experimental autoimmune encephalomyelitis (EAE).[23] To explore further the contribution of PPP2R2A in the development of systemic autoimmune disease, we crossed *B6.lpr* (lupus prone) with $dLck^{Cre}R2A^{fl/fl}$ mice to generate $B6.lpr.R2A^{fl/fl}$ (wild type) *and* $B6.lpr.dLck^{Cre}R2A^{fl/fl}$ mice in which PPP2R2A is deleted only in T cells (Figure S1A). As shown in Figures S1B–S1D, $B6.lpr.dLck^{Cre}R2A^{fl/fl}$ mice showed reduced size of thymi, decreased percentage of double-negative (DN) cells, and increased - percentage of double-positive cells in thymi as compared to those of $B6.lpr.R2A^{fl/fl}$ mice. Moreover, $B6.lpr.dLck^{Cre}R2A^{fl/fl}$ mice showed significantly reduced spleen (SPL) weight, as well as reduced size and total cell numbers in the SPL and cervical lymph nodes (CLNs) compared with $B6.lpr.R2A^{fl/fl}$ mice (Figures 1A and S1E). The percentages and numbers of T cells ($CD45^+Thy1.2^+$) in the SPLs and CLNs of $B6.lpr.dLck^{Cre}R2A^{fl/fl}$ mice were also significantly decreased compared to those of $B6.lpr.R2A^{fl/fl}$ mice (Figures 1B and 1C). Specifically, PPP2R2A deficiency in T cells significantly down-regulated the numbers of all T cell subsets, including CD4 ($Thy1.2^+CD4^+CD8^-$), CD8 ($Thy1.2^+CD4^-CD8^+$), and DN ($Thy1.2^+CD4^-CD8^-$) T cells in the SPLs and CLNs of *B6.lpr.* mice (Figure 1D). In addition, IFN-γ-($Thy1.2^+CD4^+IFN\text{-}\gamma^+$, $Thy1.2^+CD8^+IFN\text{-}\gamma^+$, and $Thy1.2^+CD4^-CD8^-IFN\text{-}\gamma^+$; Figure 1E) and IL-17A- ($Thy1.2^+CD4^+IL\text{-}17^+$, $Thy1.2^+CD8^+IL\text{-}17^+$ and $Thy1.2^+CD4^-CD8^-IL\text{-}17^+$; Figure 1F) producing cells were significantly decreased in the SPLs and CLNs of $B6.lpr.dLck^{Cre}R2A^{fl/fl}$ mice compared to those of $B6.lpr.R2A^{fl/fl}$ mice. In contrast, the percentages of the $Thy1.2^+CD4^+$ $Foxp3^+CD25^{hi}$ cells (Treg cells; Figure 1G) were significantly increased in the SPLs and CLNs of $B6.lpr.dLck^{Cre}R2A^{fl/fl}$ mice in comparison with $B6.lpr.R2A^{fl/fl}$ mice. Moreover, $B6.lpr.\ dLck^{Cre}R2A^{fl/fl}$ mice developed less lupus-like disease, as evidenced by decreased serum anti-double-stranded DNA (dsDNA) immunoglobulin G (IgG) levels (Figure 1H), proteinuria (Figure 1I), and histopathologic signs of glomerular lesions and perivascular inflammatory cell accumulation (Figures 1J and 1K) compared to those in $B6.lpr.\ R2A^{fl/fl}$ mice. Collectively, PPP2R2A deficiency in T cells protects against hallmark features of disease in lupus-prone mice.

PPP2R2A deficiency in T cells enhances NAD^+ production through the NR-directed salvage biosynthesis pathway

We had previously shown that PPP2R2A enhances Th1 and Th17 differentiation.[23] To identify mechanisms responsible for the reduction in IFN-γ- or IL-17A-producing cells in *B6.lpr* mice with T cell-specific deletion of PPP2R2A, we characterized the global metabolic consequences of PPP2R2A deficiency in naive CD4 T cells isolated from the SPLs of B6.$R2A^{fl/fl}$ *and* $B6.dLck^{Cre}\ R2A^{fl/fl}$ mice cultured under Th1 and Th17 polarization conditions for 24 h. Principal-component analysis (PCA) of the metabolomics data revealed that the metabolite profile of $R2A^{fl/fl}$ cells was clearly separated from that of $dLck^{Cre}R2A^{fl/fl}$ cells under both Th1 and Th17 polarization conditions (Figure 2A). Statistical analysis revealed that the levels of 41 and 25 metabolites were

significantly ($p < 0.1$) altered in PPP2R2A-deficient Th1 or Th17 cells, respectively (Figure 2B). Metabolite set enrichment analysis of significantly altered metabolites identified significantly ($p < 0.05$ and impact >0.1) impacted biochemical pathways, including those of glutathione metabolism, glycolysis/gluconeogenesis, nicotinate and NAM metabolism, pyruvate metabolism and terpenoid backbone biosynthesis in PPP2R2A-deficient Th1 cells, and pyrimidine metabolism, nicotinate and NAM metabolism, lysine degradation, and synthesis and degradation of ketone bodies in PPP2R2A-deficient Th17 cells (Figure 2C).

Nicotinate and NAM metabolism, which is important in the production of NAD^+, emerged in both PPP2R2A-deficient Th1 and Th17 cells (Figure 2C). Mammalian cells transport the extracellular NAD^+ precursors tryptophan (Try), nicotinic acid (NA), and NR/NAM into cells for NAD^+ biosynthesis through *de novo* synthesis, Preiss-Handler, and salvage pathways, respectively.[24–27] We made a closer examination of the metabolites involved in NAD^+ biosynthesis. As presented in Figures 3A and 3B, the levels of Try and NA were decreased in Th1, but increased in Th17 PPP2R2A-deficient cells. In addition, the level of NAM was increased in Th1, but decreased in Th17 PPP2R2A-deficient cells (Figures 3A and 3B). However, the levels of NR and its downstream metabolite NAM mononucleotide (NMN) were increased in both Th1 and Th17 PPP2R2A-deficient cells (Figures 3A and 3B). Moreover, the levels of NAD^+ or its reduced form NADH were decreased or increased in PPP2R2A-deficient Th1 cells, while increased or decreased in PPP2R2A-deficient Th17 cells (Figures 3A and 3B). Because NAD^+ and NADH are inter-converted and the concentrations measured by mass spectrometry are relative, it is difficult to conclude whether the intracellular NAD^+ levels are increased or decreased. Thus, to determine the absolute concentrations of total intracellular NAD^+ (NAD^+ and NADH) level, we used the NAD/NADH quantification kit to measure the concentration of total NAD^+ (NAD^+_{total}), including NAD^+ and NADH in $R2A^{fl/fl}$ or $dLck^{Cre}R2A^{fl/fl}$ naive CD4 T cells after culture under Th1 and Th17 polarization conditions for 24 h. As shown in Figure 3C, PPP2R2A deficiency increased the NAD^+_{total} levels in both Th1 and Th17 cells.

Since the level of NR was increased in both Th1 and Th17 PPP2R2A-deficient cells (Figures 3A and 3B), we further determined whether NR-directed NAD^+ biosynthesis through the salvage pathway plays a role in NAD^+ production in PPP2R2A-deficient or PPP2R2A-sufficient Th1 and Th17 cells. We applied vehicle (DMSO) or S-(4-nitrobenzyl)-6-thioinosine (NBTI), a small drug inhibitor of equilibrative nucleoside transporters (ENTs) that block the transport of NR from extracellular into intracellular space[28,29] during $R2A^{fl/fl}$ and $dLck^{Cre}R2A^{fl/fl}$ Th1 or Th17 cell differentiation. As shown in Figure 3D, NBTI did not significantly affect the levels of NAD^+_{total} in $R2A^{fl/fl}$ Th1 or Th17 cells compared to DMSO-treated $R2A^{fl/fl}$ Th1 or Th17 cells, suggesting that the NR-directed salvage pathway is negligible in PPP2R2A-sufficient cells. On the contrary, NBTI treatment dramatically decreased the levels of NAD_{total} in $dLck^{Cre}R2A^{fl/fl}$ Th1 or Th17 cells when compared to DMSO-treated $dLck^{Cre}R2A^{fl/fl}$ counterparts (Figure 3D). Metabolomics analysis of extracellular metabolites showed that NBTI treatment blocked the uptake of NR as evidenced by the increased extracellular levels of NR when compared to DMSO-treated PPP2R2A-deficient T cells (Figure S2). These data signify the importance of the NR-directed salvage pathway in the biosynthesis of NAD^+ in PPP2R2A-deficient T cells. We further performed qPCR analysis to determine the levels of NAD^+ biosynthetic

enzymes to determine whether PPP2R2A deficiency affects their expression. PPP2R2A deficiency significantly enhanced the mRNA expression levels of *Nmrk1* (NRK1), *Nmrk2* (NRK2), *Nmnat1*, *Nmnat2*, and *Nmnat3* (Figure 3E), which are the key enzymes involved in the NR-directed NAD^+ biosynthesis salvage pathway (Figure 3B) in both Th1 and Th17 cells. However, PPP2R2A deficiency did not significantly affect the level of *Nampt*, which is the rate-limiting enzyme in the NAM-mediated NAD^+ salvage pathway (Figure 3B). Moreover, the mRNA levels of *Nadsyn1* (NADS), which catalyzes the conversion of nicotinic acid adenine dinucleotide (NAAD) to NAD^+ in *de novo* synthesis and the Preiss-Handler pathway (Figure 3B) was down-regulated in PPP2R2A-deficient Th1 and Th17 cells compared to PPP2R2A-sufficient counterparts (Figure 3E). Collectively, these results confirm that PPP2R2A deficiency increases NAD^+ levels through the NR-directed NAD^+ biosynthesis salvage pathway in both Th1 and Th17 cells.

NR inhibits Th1 and Th17 cell differentiation but augments Treg cell differentiation *in vitro*

To investigate whether NAD^+ is essential for *in vitro* T cell differentiation, we isolated naive $CD4^+$ T cells from the SPLs of $R2A^{fl/fl}$ mice and cultured them under Th1-, Th17-, and Treg-polarizing conditions in the presence of PBS or NR (500 μM) for 72 h *in vitro*. As presented in Figures 4A and 4B, NR treatment significantly reduced the percentages of IFN-γ (Th1)- and IL-17 (Th17)-producing cells. Surprisingly, NR treatment enhanced Foxp3-expressing cells (Treg cells; Figures 4A and 4B). As expected, NR treatment significantly up-regulated intracellular NAD^+ levels in these cell subsets (Figure 4C), and NBTI significantly blunted NR-induced intracellular NAD^+ levels (Figure 4D). Furthermore, NR treatment significantly down-regulated the mRNA expression level of *Ifng* and *Tbx21* (T-bet) in Th1 cells (Figure 4E), suggesting that NR inhibited Th1 cell differentiation by down-regulating the Th1 master transcription factor T-bet. However, NR treatment significantly reduced the mRNA expression levels of *Il17a*, but not *Rorc* and *Stat3* in Th17 cells (Figure 4F), and increased the levels of *Foxp3*, but not *Cd25* and *Stat5a* in Treg cells (Figure 4G). Moreover, NR treatment did not induce significant changes in the levels of p-Stat3 in Th17 cells (Figure 4H) and p-Stat5 in Treg cells (Figure 4I). These results indicate that NR treatment inhibited Th17 cell polarization but augmented Foxp3 expression independently of the Stat3/Stat5 pathway.

NR treatment alters the occupancy of histone H1 in Il17a and Foxp3 loci

We next interrogated the mechanism whereby NR treatment inhibited IL-17 but augmented Foxp3 expression. NAD^+ can directly participate in protein modification by serving as a substrate of NAD^+-consuming enzymes including two major families, sirtuins and poly (ADP-ribose) polymerases (PARPs).[24–27] Sirtuins use NAD^+ as a co-substrate to remove acetyl moieties from lysine residues, resulting in protein deacetylation.[24–27] Active PARPs (mainly PARP1) catalyze the transfer of ADP-ribose subunits from NAD^+ to protein acceptors, a process called poly-ADP-ribosylation (PAR) or PARylation.[24–27] Interestingly, NR treatment dramatically increased the levels of PARylated proteins (Figures 5A and S3B), while it did not significantly affect the levels of acetylated proteins (Figures S3A and S3B) in Th17 and Treg cells, implying that protein PARylation may play an important role in the NR-induced inhibition of IL-17 expression and augmentation of Foxp3 expression. In addition, PARP1 autoPARylation, which enhances PARP1 enzymatic activity,[30] was

increased in both NR-treated Th17 and Treg cells as compared to PBS-treated counterparts (Figure 5A). Moreover, NBTI blunted NR-induced PAR in both Th17 and Treg cells (Figure S3C), consistent with the finding presented in Figure 4D. Interestingly, PPP2R2A deficiency increased the level of PAR, which was blocked by NBTI in CD4 T cells stimulated with anti-CD3/CD28 (Figure S3D). To determine which proteins were extensively PARylated, we performed immunoprecipitation (IP)-mass spectrometry (MS) analysis of PARylated proteins from naive CD4 T cells after culture under Treg cell differentiation conditions for 24 h in the presence of PBS or NR (Figure S3E). This analysis detected 2,563 PARylated proteins in PBS- and NR-treated Treg cells, and statistical evaluation identified significantly (|log2 fold change| > 2) altered PARylated levels in 24 proteins with increased and 26 proteins with decreased PARylation in NR-treated Treg cells compared to PBS-treated Treg cells (Figure 5B). Gene Ontology (GO) pathway analysis of these significantly altered PARylated proteins showed that negative regulation of DNA recombination, chromosome condensation, nucleosome organization, and chromatin organization biological processes was impacted significantly (Figure 5C). Specifically, three subtypes (H1.4, H1.2, and H1.5) of the histone H1 protein family were involved in these processes, and their PARylation was up-regulated in NR-treated Treg cells (Figures 5B and 5C). Histone H1, especially the H1.2 subtype, regulates the epigenetic landscape by local chromatin compaction,[31] and PARylation changes its occupancy of chromatin domains.[32,33]To further confirm H1.2 PARylation in Th17 and Treg cells, we pulled down H1.2 using an antibody against H1.2 and detected the PARylated H1.2 by western blot analysis using a PAR antibody, because a PARylated H1.2 antibody is not available. As presented in Figures 5D, S3F, and S3G, NR treatment increased the level of PARylated H1.2 in both Th17 and Treg cells, which is consistent with the finding by MS analysis. Intriguingly, PARylated H1.2 was increased in PPP2R2A-deficient as compared to PPP2R2A-sufficient CD4 T cells stimulated by anti-CD3/CD28 (Figure S3H). It is reported that the promoter-defined conserved noncoding sequences (CNS) 1 and CNS2 in the *Foxp3* gene locus are required for *Foxp3* gene transcription in Treg cells.[34] In addition, CNS2 in the *Il17a* gene locus is sufficient and necessary for *Il17a* gene transcription in Th17 cells.[35] We next asked whether NR treatment affects the occupancy of H1.2 in these regions. Chromatin IP (ChIP)-qPCR experiments revealed that NR treatment decreased the binding of H1.2 to the promoter CNS1 and CNS2 regions in the *Foxp3* gene locus but that they increased the enrichment of H1.2 in the CNS2 region within the *Il17a* gene locus in both Treg and Th17 cells (Figure 5E). In contrast, NR treatment led to the accumulation of H3K36m2, which is associated with increased gene transcription in the CNS1 and CNS2 regions within the *Foxp3* gene locus in Treg cells, but reduced the binding of H3K36m2 to the CNS2 region within the *Il17a* gene locus in Th17 cells (Figure 5F). Collectively, NR treatment reduced the occupancy of histone H1 protein in the *Foxp3* gene locus but increased the occupancy in the *Il17a* gene locus, promoting *Foxp3* gene transcription but decreasing *Il17a* gene transcription.

NR treatment suppresses lupus-related disease in MRL.lpr mice

To determine the role of NR in the regulation of lupus-associated pathology, we injected intraperitoneally PBS or NR Cl (NR chloride, 500 mg/kg body weight/day) into 8-week-old *MRL.lpr* (lupus prone) mice daily for 9 weeks (Figure S4A). *MRL.mpj* mice injected with PBS were used as the control. As shown in Figures 6A and S4B, NR

Cl-treated *MRL.lpr* mice showed significantly reduced SPL weight and SPL and CLN size, and the cell numbers compared with PBS-treated *MRL.lpr* mice. The percentages and numbers of T cells ($CD45^+Thy1.2^+$) in SPLs and CLNs of NR-treated *MRL.lpr* mice were significantly decreased compared to those of PBS-treated *MRL.lpr* mice (Figures 6B and 6C). Specifically, NR Cl treatment down-regulated significantly the numbers of all T cell subsets, including CD4 ($Thy1.2^+CD4^+CD8^-$), CD8 ($Thy1.2^+CD4^-CD8^+$), and DN ($Thy1.2^+CD4^-CD8^-$) T cells in the SPLs and CLNs of *MRL.lpr* mice (Figure 6D). Ki67 expression of T cells ($CD45^+Thy1.2^+$) in the SPLs and CLNs of NR Cl-treated *MRL.lpr* mice was significantly lower than in PBS-treated *MRL.lpr* mice, implying that NR Cl treatment significantly reduced T cell proliferation (Figures S4C and S4D). NR Cl treatment, however, did not affect the body weight of *MRL.lpr* mice compared to PBS-treated *MRL.lpr* mice (Figure S4E). Treatment significantly decreased IFN-γ-producing ($Thy1.2^+CD4^+IFN\text{-}\gamma^+$, $Thy1.2^+CD8^+IFN\text{-}\gamma^+$, and $Thy1.2^+CD4^-CD8^-IFN\text{-}\gamma^+$; Figure 6E) and IL-17A-producing ($Thy1.2^+CD4^+IL\text{-}17^+$, $Thy1.2^+CD8^+IL\text{-}17^+$, and $Thy1.2^+CD4^-CD8^-IL\text{-}17^+$; Figure 6F) cells in the SPLs and CLNs of NR-treated *MRL.lpr* mice compared to PBS-treated *MRL.lpr* mice. In contrast, the percentages of the $Thy1.2^+CD4^+Foxp3^+CD25^{hi}$ Treg cells (Figure 6G) were significantly increased in the NR Cl-treated *MRL.lpr* mice in comparison with the PBS-treated *MRL.lpr* mice. Moreover, NR Cl-treated *MRL.lpr* mice developed less nephritis, as evidenced by the decreased anti-dsDNA IgG levels in the serum (Figure 6H), proteinuria (Figure 6I), and histopathologic signs of glomerular and tubular lesions and perivascular cell accumulation (Figures 6J and 6K) when compared with PBS-treated *MRL.lpr* mice. Western blot analysis of protein lysates extracted from the splenocytes of mice showed that treatment with NR Cl increased PARylated PARP1 but decreased the cleaved PARP1 in the splenocytes of *MRL.lpr* mice (Figure S4F), signifying that PARP1 was activated in *MRL.lpr* mice after NR Cl treatment. Collectively, NR Cl treatment suppresses disease in lupus-prone mice.

NR supplementation restores PARP1 activity and reduces IFN-γ and IL-17 expression in CD4 T cells from patients with SLE

Low PARP1 enzymatic activity has been reported in peripheral blood mononuclear cells (PBMCs) from patients with SLE.[36] PARP1 is involved in DNA repair, inflammation, and cell death, and it enhances its enzymatic activity in autoPARylation,[30] whereas it loses its activity once cleaved.[37,38] To determine the translational value of our findings, we compared the PARP1 activity of CD4 T cells from healthy control subjects and patients with SLE (Table 1) by determining the levels of PARylated and cleaved PARP1. As presented in Figures 7A and 7B, PARP1 autoPARylation was significantly decreased, whereas the cleavage of PARP1 into multiple fragments was at significantly higher levels in CD4 T cells from patients with SLE as compared to those in CD4 T cells from race-, age-, and sex-matched healthy subjects. This finding suggests that CD4 T cells from patients with SLE have low PARP1 enzymatic activity. Moreover, culture of SLE $CD4^+$ T cells in the presence of NR led to a significant increase in PARylated PARP1 and PAR, but it did not affect the cleaved PARP1 (Figures 7C and 7D), suggesting that PARP1 activity was enhanced. Moreover, the mRNA expression levels of *IFNG and IL17A* were decreased after supplementation with NR (Figure 7E). Collectively, these results demonstrate that

NR supplementation can restore PARP1 enzymatic activity and reduce IFN-γ and IL-17 expression in CD4 T cells from patients with SLE.

DISCUSSION

In this communication, we present evidence that PPP2R2A, a regulatory subunit of PP2A, is needed for the development of systemic autoimmunity, and its genetic absence in T cells limits disease expression. While deciphering the involved mechanisms, we fortuitously found that this regulatory subunit controls the entry of NR into the cells and NAD^+ biosynthesis through the salvage pathway, and it regulates T cell differentiation by PARylating histone H1.2, leading to its differential occupancy of regulatory regions of the *Foxp3* and *Il17a* loci. At the translational level, NR treatment prevented systemic autoimmunity in *MRL.lpr* mice and decreased IFN-γ and IL-17 production in CD4 T cells from patients with SLE.

SLE is an autoimmune disorder that is characterized by diverse T effector cell dysfunction involving increased cytokine production such as IL-17 and IFN-γ, which may contribute directly to organ inflammation.[1–3,4] IL-17, a proinflammatory cytokine, is produced rapidly and in large amounts by $CD4^+$, $\gamma\delta^+$, and $CD4^-CD8^-$ (DN) $TCR\alpha\beta^+$ T cells[39–41] that are present in the periphery and in the kidney tissue of patients with lupus nephritis.[41] We had previously found that PPP2R2A was upregulated in T cells from patients with SLE and EAE, and genetic PPP2R2A deficiency in murine T cells reduced Th1 and Th17 differentiation.[23] In the present study, using a lupus-prone mouse, we demonstrate that mice with PPP2R2A deletion only in T cells produced less IL-17- and IFN-γ-producing T cells and developed less lupus-like glomerulonephritis, signifying that PPP2R2A is a promising therapeutic target for lupus-related organ inflammation.

T cells reprogram their metabolism to support their energetic demands according to their activation status.[5] For example, Th1 and Th17 cells utilize mainly aerobic glycolysis and glutaminolysis, while naive CD4 T cells and Treg cells primarily use fatty acid oxidation and oxidative phosphorylation.[6] T cells from patients with SLE exhibit significant metabolic abnormalities[7] that can alter gene expression by modulating the epigenetic landscape[8] and promote the differentiation of T cells toward proinflammatory subsets such as Th1 and Th17 cells.[8] In the present study, we have identified that NAD^+ metabolism is significantly impacted in T cells subjected to Th1 and Th17 cell polarization conditions when PPP2R2A expression is absent. Specifically, PPP2R2A deficiency increased NAD^+ levels when T cells were cultured under proinflammatory conditions. This finding implies that the increased NAD^+ levels in PPP2R2A-deficient cells probably account for the reduced ability of PPP2R2A-deficient naive CD4 T cells to differentiate into Th1 and Th17 cells.[23] Indeed, Th1 and Th17 cell differentiation was significantly reduced after we supplemented the cell medium with NR to boost intracellular NAD^+ levels. Mammalian cells use NAD^+ precursors Try, NA, and NR/NAM to synthesize NAD^+ through *de novo* synthesis, Preiss-Handler, and salvage pathways, respectively.[24–27] Our data reveal that blockage of the NR-directed pathway did not significantly affect intracellular NAD^+ levels in PPP2R2A-sufficient cells but caused a dramatic down-regulation of NAD^+ levels in PPP2R2A-deficient cells, suggesting that the NR-directed salvage pathway is negligible in PPP2R2A-sufficient

cells, while PPP2R2A-deficient cells rewire the NR-directed salvage pathway to boost intracellular NAD^+. The fact that PPP2R2A deficiency inhibited the metabolic enzyme involved in *de novo* synthesis and Preiss-Handler pathways while it enhanced the expression of enzymes that contribute to the NR-mediated salvage pathway indicates that PPP2R2A is vital in the regulation of NAD^+ metabolism in T cells. Thus, PPP2R2A, which was found up-regulated in SLE T cells,[23] represents one of the factors that drive metabolic abnormalities in T cells.

NAD^+ is not only an essential cofactor for multiple cellular redox processes linked to fuel utilization and energy metabolism but it is also a substrate for multiple enzymes such as sirtuins and PARPs to regulate signaling pathways, post-translational modifications, epigenetic changes, and RNA stability and function.[24–27] NAD^+ levels decline during aging, and alterations in NAD^+ homeostasis can be found in virtually all age-related diseases, including neuro-muscular, cardiometabolic, liver, and kidney diseases.[24,25] For this reason, the therapeutic and preventive potential of NAD^+ boosting has been scrutinized in a variety of preclinical models and disease settings.[24,25] In patients with SLE, cellular NAD^+ levels were found to be low in CD8 T cells due to the increased expression of CD38[42] and high IFN signaling.[43] Replenishment of cellular NAD^+ levels using either a CD38 inhibitor[44] or NMN[43] restored the cytotoxicity of CD8 T cells. NR has been used widely to boost intracellular NAD^+ levels [45] and is transported into the cell via SLC29A1.[28] NR can be either directly administered or from the conversion of NAD^+, NAM, or NMN by CD73 extracellularly.[24–27] Previously, NR was found to reduce autophagy and type I IFN signaling in monocytes from patients with SLE and can be used as a potential adjunct to treat SLE patients.[46] In this study, we provide evidence that the administration of NR in *MRL.lpr* mice decreased the numbers of IL-17- and IFN-γ-producing T cells, increased the percentage of Treg cell population, and reduced the development of lupus nephritis. In addition, low PARP1 enzymatic activity has been reported in PBMCs from patients with SLE.[36] In the present report, we demonstrate that PARP1 autoPARylation, which promotes its enzymatic activity,[30] was decreased in CD4 T cells from patients with SLE, while supplementation with NR increased the level of PARylated PARP1 and reduced IFN-γ and IL-17 production. These findings provide rationale to use NR to treat patients with SLE.

Th17 cells that produce IL-17, IL-22, and IL-23 and Treg cells that produce anti-inflammatory cytokines play opposite roles in the regulation of the inflammatory immune response.[47] Patients with SLE have increased numbers of Th17 cells[41,48] but decreased numbers of Treg cells[2] in both peripheral blood and tissues. Stat3/RORyt signaling is critical for Th17 cell differentiation,[49,50] while development and differentiation of Treg cells and expression of Foxp3 depend on another transcription factor, Stat5.[51,52] We found that NR treatment inhibits Th17 cell differentiation and IL-17 expression independently of Stat3/RORyt signaling, but enhanced Treg cell differentiation and Foxp3 expression without affecting the expression of the transcription factor Stat5. NAD^+ can participate directly in protein modification, and modulate chromatin structure and gene transcription through PARP1.[53] In agreement with this thesis, we identified many PARylated proteins that are involved in the chromatin organization process after NR treatment, including increased levels of PARylated histone 1.2. Specifically, we found that histone H1 displayed increased occupancy in the *Il17a* locus and decreased occupancy in the *Foxp3* locus after

NR treatment. It is reported that H1 histones can regulate gene transcription by controlling the epigenetic landscape in T cells.[31] Here, we provide evidence that modulation of histone H1.2 by NR alters its occupancy in *Il17a* and *Foxp3* loci to control their transcription.

In summary, we have shown that PPP2R2A, a regulatory subunit of PP2A, regulates NAD^+ metabolism, and its specific targeting increases NAD^+ production and decreases Th1/Th17 cell differentiation in autoimmune diseases. Importantly, administration of NR to lupus-prone mice increased NAD^+ levels and suppressed autoimmunity and nephritis, whereas culture of CD4 T cells from patients with SLE in the presence of NR decreased IFN-γ and IL-17 production. NR is orally bioavailable[54] and reduces levels of circulating inflammatory cytokines in humans,[55] and accordingly, patients with autoimmune diseases should benefit from NR supplementation.

Limitations of the study

Our study has several limitations. For instance, in the polar metabolomics profiling, only 303 metabolites were examined. Although these 303 metabolites participated in the bulk of the metabolic processes, the measured metabolites in each pathway were limited. Although we are able to assign metabolites into specific pathways, it is possible that others belonging to other pathways were not measured. Another limitation has to do with the experiments in mice. Although we used MRL.*lpr* mice to treat with NR Cl, genetic deletion of *Ppp2r2a* in T cells was performed in B6.*lpr* mice. It is known that *MRL.lpr* mice display more severe autoimmunity and pathology than *B6.lpr* mice.[56,57] Thus, we may have recorded a differential effect between PPP2R2A deletion specific in T cells and NR treatment on lupus pathology possibly because the *B6.lpr* mice develop milder disease than do the *MRL.lpr* mice. In addition, we used Lck^{Cre} to delete PPP2R2A expression only in T cells rather than other cell types. However, NR Cl administration into mice by intraperitoneal injection could affect not only T cells but also other cell subsets. It has been reported[46] that NR reduces autophagy and type I IFN signaling in monocytes from patients with SLE. Finally, the effect of NR on other immune cell subsets is currently largely unknown.

STAR★METHODS

RESOURCE AVAILABILITY

Lead contact—Further information and requests for resources and reagents should be directed to and will be fulfilled by the lead contact, George C. Tsokos (gtsokos@bidmc.harvard.edu).

Materials availability—*$R2A^{fl/fl}$ or $dLck^{Cre}R2A^{fl/fl}$* mice in B6, or B6.lpr background are available from the lead contact upon request.

Data and code availability

- All data reported in the paper are available from the lead contact upon request.
- This paper does not report original code.

- Any additional information required to reanalyze the data reported in this paper is available from the lead contact upon request.

EXPERIMENTAL MODEL AND STUDY PARTICIPANT DETAILS

Mice—PPP2R2A-flox ($R2A^{fl/fl}$) and $dLck^{Cre}R2A^{fl/fl}$ mice in which PPP2R2A is deleted in T cells were generated as previously described.[23] In the current study, we crossed *B6.MRL-Faslpr/J* (*B6.lpr*, The Jackson Laboratory, Stock No: 000482) with $Lck^{Cre}R2A^{fl/fl}$ mice to generate $B6.lpr.R2A^{fl/fl}$ (wild-type) *and* $B6.lpr.Lck^{Cre}R2A^{fl/fl}$ mice where PPP2R2A is deleted only in T cells. To dissect the role of PPP2R2A in the development of systemic lupus erythematosus-like autoimmune disease, twenty-six-weeks-old $B6.lpr.R2A^{fl/fl}$ *and* $B6.lpr.dLck^{Cre}R2A^{fl/fl}$ sex-matched littermates were used to study lymphoproliferation. For renal pathology, thirty-five-weeks-old sex-matched littermates were used. *MRL/MpJ-Faslpr/J* (*MRL.lpr*, Stock No: 000485) and *MRL/MpJ* (Stock No: 000485) mice were purchased from The Jackson Laboratory. To determine the role of nicotinamide riboside chloride (NR Cl, TruNiagen, ChromaDex) in the regulation of lupus-related pathology, we injected intraperitoneally PBS or NR (500 mg/kg body weight/day) into 8-weeks-old *MRL.lpr* mice daily for 9 weeks. *MRL.mpj* mice injected with PBS were used as lupus-related disease-free control. All mice were bred and housed in a specific pathogen-free environment in a barrier facility in accordance with the Beth Israel Deaconess Medical Center Institutional Animal Care and Use Committee (IACUC).

Patients enrolled in the study and CD4 T cell isolation and stimulation—A total of 24 patients with systemic lupus erythematosus and age-, sex-, and ethnicity-matched 14 healthy donors were enrolled in this study. Primary CD4 T cells were purified from peripheral venous blood obtained from healthy volunteers as well as patients. The blood was incubated for 30 min with a rosette CD4 T cell purification kit (Stem Cell Technologies). Lymphocyte separation medium (17-829E, Lonza) was subsequently used to separate these complexes from CD4 T cells. For stimulation, CD4 T cells were cultured in RPMI 1640 medium, (10-040-CVR, Corning), 10% heat-inactivated FBS (SH3007003HI, Hyclone), 2 mM glutamine (25-030-081, Gibco, Thermo Fisher Scientific), 100 U/mL penicillin, and 100 μg/mL streptomycin (15140122, Thermo Fisher Scientific) at 37°C, 5% CO2. CD4 T cells were stimulated with plate-bound OKT3/anti-CD3 (5 μg/mL, 317325, BioLegend) and anti-CD28 (1 μg/mL, CD28.2, BioLegend) in the presence or absence of NR (500 μM) for the indicated time.Studies were approved by the Institutional Review Board of Beth Israel Deaconess Medical Center (BIDMC).

Study approval—Human samples study (protocol 2006-P-0298) was approved by BIDMC IRB. Informed consent was obtained from all study subjects. All animal procedures were approved by the IACUC of BIDMC, Harvard Medical School. All mice were maintained in an SPF animal facility (BIDMC). All mice were genotyped to validate claimed strain.

METHOD DETAILS

***In vitro* T cell differentiation—**Naive $CD4^+$ T cells were purified by mouse $CD4^+CD62L^+$ T cell Isolation Kit II (Miltenyi Biotec). Purified naive T cells were

stimulated with plate-bound goat anti-hamster IgG (SKU 0856984, MP Biomedicals), soluble anti-CD3 (0.25 μg/mL,145-2C11; BioLegend), and anti-CD28 (0.5 μg/mL, 37.51; BioLegend) for Th0-nonpolarized condition culture. In addition to Th0-nonpolarized condition, the following stimulation was used for each polarized condition: IL-12 (20 ng/mL; R&D Systems) and anti-IL-4 (10 μg/mL, C17.8; BioLegend) for Th1; IL-6 (3 ng/mL; R&D Systems), TGF-β1 (0.3 ng/mL; R&D Systems), anti–IL-4 (10 μg/mL, C17.8; BioLegend), and anti–IFN-γ (10 μg/mL; XMG1.2; BioLegend) for Th17; and IL-2 (20 ng/mL; R&D Systems), TGF-β1 (3 ng/mL), anti–IL-4 (10 μg/mL), and anti–IFN-γ (10 μg/mL) for Treg. In addition to antibodies and cytokines, in some experiments, cells were cultured in the presence of PBS or NR (500 μM, HB-5832, Combi-Blocks).

Mass spectrometry

Polar metabolomics profiling: Metabolites were extracted from cells or culture medium using 80% methanol (v/v). Polar metabolomics profiling (303 metabolites) was performed by using liquid chromatography-tandem mass spectroscopy (LC/MS) in the BIDMC mass spectrometry core according to the protocol.[58] Once the SRM data were acquired, peaks were integrated in order to generate chromatographic peak areas used for quantification across the sample set. Metabolomics data were analyzed using MetaboAnalyst 5.0 (http://www.metaboanalyst.ca/).[59] Briefly, missing metabolite raw intensity values were filled in with the lowest detectable intensity of the respective metabolites, and all raw intensities were normalized to the sum intensity of the respective replicate, mean-centered and divided by the standard deviation of each variable. Metabolites between groups were identified and subjected to principal component analysis (PCA), statistical analysis (*t* test) and enrichment analysis.

Protein identification: In order to identify PolyADP-ribosylated protein, we performed immunoprecipitation-mass spectrometry (IP-MS) analysis. Briefly, protein lysate was digested by TPCK modified trypsin (1 μg/μL) overnight at 37°C with shaking 250 rpm. Peptides were then purified by loading samples onto reversed-phase C18 cartridges (SepPak Classic, 360 mg sorbent, 0.85 mL, Waters) and lyophilized. The dried peptides were then dissolved with IP buffer and incubated with antibody against PAR/pADPr (Clone # 10HA, 4335-MC-100, R&D Systems) for IP experiments using Dynabeads Protein G Immunoprecipitation Kit (Thermo Fisher Scientific) according to manufacturer's instructions. The antibody-bound peptides were then purified and subjected to LC/MS analysis for identification of peptide/protein in the BIDMC mass spectrometry.

NAD/NADH quantification—The total intracellular NAD levels (NAD+ and NADH) were determined using NAD/NADH Quantitation Kit (MAK037, Sigma-Aldrich) following manufacture's instructions.

Quantitative (q) PCR—Total RNA was isolated from purified T cells with RNeasy Plus Micro Kit (QIAGEN). The isolated RNA was transcribed into cDNA using the RNA to cDNA premix (Clontech) according to the manufacturer's instructions. SYBR green was purchased from Roche, and the assays were performed on 96-well reaction plates (Invitrogen). The real-time PCR was performed on LightCycler 480 device (Roche). In all

experiments, β-actin was used as reference gene to normalize gene expression and ΔΔCT method was used to calculate the fold change of target gene expression. The primers used are shown in Table S1.

Western blotting—Cell lysates were prepared using RIPA buffer (Boston BioProducts) containing protease cocktail inhibitor (cOmplete Mini EDTA-free, Roche) and phosphatase cocktail inhibitor (PhosSTOP, Roche). Protein concentration was determined by Coomassie protein assay reagent (MilliporeSigma). Total protein (30 μg) was resolved by a NuPAGE 4%–12% Bis-Tris gel (Invitrogen), and transferred to PVDF membrane (Thermo Fisher Scientific). After blocking with 5% nonfat milk (M-0841, LabScientific), the membrane was incubated with primary antibody overnight at 4°C. Subsequently, the membrane was incubated with secondary antibody for 90 min at room temperature. Western ECL substrate (1705061, Bio-Rad) was used to develop the immunoblot. The picture was captured and analyzed by Image Lab (Version 5.2.1) using ChemiDoc XRS+ System (Bio-Rad). Primary antibodies against PARP1 (sc-7150, Santa Cruz Biotechnology), PAR (4335-MC-100, R&D Systems), and β-actin (A5316, Sigma-Aldrich), and goat anti-mouse IgG (H + L) secondary antibody (31430, Thermo Fisher Scientific) and goat anti-rabbit IgG (H + L) secondary antibody (31460, Thermo Fisher Scientific) were used. The results were quantified by plotting the intensity of the band. β-actin was used as the loading control.

Flow cytometry—Cells were stained with fluorescence-tagged antibodies purchased from eBioscience, BD Biosciences, Tonbo Bioscience, or BioLegend (Table S2), and analyzed using Cytoflex flow cytometer. Flow cytometry data were analyzed using CytExpert version 2.0 of Flowjo. For intracellular cytokine staining, cells were stimulated with 50 ng/mL of PMA, 1 μM of ionomycin, and 1 μg/mL of brefeldin A for 4 h in the presence of brefeldin A; they were then harvested, fixed, and stained with BD Cytofix/Cytoperm Fixation/Permeabilization Solution Kit. For cell sorting, FACSAria (BD) was used and the purity of the sorted population was over 95%.

Chromatin immunoprecipitation (ChIP)-qPCR—ChIP experiments were performed with the MAGnify Chromatin Immunoprecipitation System (49–2024; Life Technologies) following the manufacturer's instructions. Briefly, 1×10^6 cells were cross-linked with 1% formaldehyde for 10 min at room temperature. The reaction was stopped with glycine for 5 min, and the samples were lysed and sonicated to obtain 200- to 500-bp fragments. Immunoprecipitation was performed with an H1.2 antibody (JU43-48, NBP2-75932, Novus Biologicals), H3K36m2 (07–274, Millipore-Sigma) or an IgG control (49–2024; Life Technologies). Cross-linking was reversed, and DNA was eluted and purified using DNA-purification magnetic beads. Enrichment for the mouse *Foxp3 promoter*, *CNS1* and *CNS2,* and *Il17a CNS2* genomic sequence in the samples was quantified by real-time qPCR and was normalized with the input samples. The primers used are shown in Table S1.

Renal histopathology—Hematoxylin-Eosin- and Periodic acid-Schiff (PAS)-stained paraffin sections of formalin-fixed kidneys from each mouse were assessed blindly for glomerular lesions (hypercellularity, exudates, hyalinosis, necrosis, crescent formation), tubular lesions (atrophy, dilation, necrosis, casts) and perivascular mononuclear cell

accumulation. Glomerular lesions and perivascular cell accumulations were scored on a scale of 0–3, and tubular lesions were scored as percentage of cortical tubule involvement, as previously described.[60]

Enzyme-linked immunosorbent assay (ELISA)—dsDNA antibody levels were measured using a homemade enzyme-linked immunosorbent assay as previously described.[61] Briefly, sera were diluted 1:50 with 1% PBS bovine serum albumin and incubated at room temperature with shaking for 2 h on 96-well plates precoated with l-lysin (0.05 mg/mL) for 2 h at room temperature, then coated with Calf thymus DNA (0.1 mg/mL, Sigma-Aldrich) at 4°C overnight. Standard was made using serial dilution of the serum of one 16-week-old MRL/lpr mouse. After washing, the wells were incubated with an alkaline phosphatase–conjugated goat anti-mouse immunoglobulin G antibody (1:5000; Jackson ImmunoResearch) for 1 h, and colorimetric reaction was provoked by adding diethanolamine substrate buffer (Thermo Fisher Scientific) and PNPP (*p*-Nitrophenyl Phosphate)-phosphatase substrate (Sigma-Aldrich) and read at 405 nm. The results are expressed as units per volume.

Immunoprecipitation (IP)—IP experiments were conducted using Dynabeads Protein G Immunoprecipitation Kit (Thermo Fisher Scientific) according to manufacturer's instructions. Briefly, protein lysates were prepared using ice-cold IP lysis buffer containing protease cocktail inhibitor (cOmplete Mini EDTA-free, Roche) and phosphatase cocktail inhibitor (PhosSTOP, Roche). Then, the mixture magnetic beads/antibody either against H1.2 (JU43-48, NBP2-75932, Novus Biologicals) or normal rabbit IgG (s49-2024; Life Technologies) as indicated was made by 10 min at room temperature under continuous mixing. Then beads/antibody mixture was then incubated with protein lysate overnight at 4°C. The beads were then collected on a magnetic stand and washed, and the protein complex was eluted from the beads for Western blot analysis.

QUANTIFICATION AND STATISTICAL ANALYSIS

Western blots were quantified by plotting the intensity of the band using Image Lab (Bio-rad). β-actin was used as the loading control. Flow cytometry data was analyzed by Flowjo or CytoExpert 2.0. SLE is an autoimmune disease with a complex pathogenesis. In addition, even healthy people of different age, sex, or ethnicity have variable T cell numbers and function. In order to mitigate this variability, we paired each SLE patient to age-, sex-, and ethnicity-matched healthy control in order to exclude the differences caused by age-, sex-, and ethnicity. All statistical analyses were conducted using GraphPad Prism 7 (GraphPad software Inc.). Data were presented as mean ± SD. Statistical differences between 2 populations were calculated by *t* test (2-tailed) including multiple *t* test, unpaired *t* test, or paired *t* test. For multiple populations' comparison, two-way ANOVA with Turkey's multiple-comparisons test was used. $p < 0.05$ was considered statistically significant.

Supplementary Material

Refer to Web version on PubMed Central for supplementary material.

ACKNOWLEDGMENTS

This work was supported by NIH grants R01 AI136924 and R01 AI085567.

REFERENCES

1. Liu Z, and Davidson A (2012). Taming lupus-a new understanding of pathogenesis is leading to clinical advances. Nat. Med 18, 871–882. 10.1038/nm.2752nm. [PubMed: 22674006]
2. Moulton VR, and Tsokos GC (2015). T cell signaling abnormalities contribute to aberrant immune cell function and autoimmunity. J. Clin. Invest 125, 2220–2227. 10.1172/JCI78087. [PubMed: 25961450]
3. Tsokos GC (2011). Systemic lupus erythematosus. N. Engl. J. Med 365, 2110–2121. 10.1056/NEJMra1100359. [PubMed: 22129255]
4. Beringer A, Noack M, and Miossec P (2016). IL-17 in Chronic Inflammation: From Discovery to Targeting. Trends Mol. Med 22, 230–241. 10.1016/j.molmed.2016.01.001. [PubMed: 26837266]
5. Pearce EL, and Pearce EJ (2013). Metabolic pathways in immune cell activation and quiescence. Immunity 38, 633–643. 10.1016/j.immuni.2013.04.005. [PubMed: 23601682]
6. Kono M, Yoshida N, and Tsokos GC (2020). Metabolic control of T cells in autoimmunity. Curr. Opin. Rheumatol 32, 192–199. 10.1097/bor.0000000000000685. [PubMed: 31842032]
7. Morel L (2017). Immunometabolism in systemic lupus erythematosus. Nat. Rev. Rheumatol 13, 280–290. 10.1038/nrrheum.2017.43. [PubMed: 28360423]
8. Oaks Z, and Perl A (2014). Metabolic control of the epigenome in systemic Lupus erythematosus. Autoimmunity 47, 256–264. 10.3109/08916934.2013.834495. [PubMed: 24128087]
9. Vyshkina T, Sylvester A, Sadiq S, Bonilla E, Canter JA, Perl A, and Kalman B (2008). Association of common mitochondrial DNA variants with multiple sclerosis and systemic lupus erythematosus. Clin. Immunol 129, 31–35. 10.1016/j.clim.2008.07.011. [PubMed: 18708297]
10. Yu X, Wieczorek S, Franke A, Yin H, Pierer M, Sina C, Karlsen TH, Boberg KM, Bergquist A, Kunz M, et al. (2009). Association of UCP2 –866 G/A polymorphism with chronic inflammatory diseases. Genes Immun 10, 601–605. 10.1038/gene.2009.29. [PubMed: 19387457]
11. Yin Y, Choi SC, Xu Z, Perry DJ, Seay H, Croker BP, Sobel ES, Brusko TM, and Morel L (2015). Normalization of CD4+ T cell metabolism reverses lupus. Sci. Transl. Med 7, 274ra18. 10.1126/scitranslmed.aaa0835.
12. Bednarski JJ, Warner RE, Rao T, Leonetti F, Yung R, Richardson BC, Johnson KJ, Ellman JA, Opipari AW Jr., and Glick GD (2003). Attenuation of autoimmune disease in Fas-deficient mice by treatment with a cytotoxic benzodiazepine. Arthritis Rheum 48, 757–766. 10.1002/art.10968. [PubMed: 12632430]
13. Kono M, Yoshida N, Maeda K, and Tsokos GC (2018). Transcriptional factor ICER promotes glutaminolysis and the generation of Th17 cells. Proc. Natl. Acad. Sci. USA 115, 2478–2483. 10.1073/pnas.1714717115. [PubMed: 29463741]
14. Johnson MO, Wolf MM, Madden MZ, Andrejeva G, Sugiura A, Contreras DC, Maseda D, Liberti MV, Paz K, Kishton RJ, et al. (2018). Distinct Regulation of Th17 and Th1 Cell Differentiation by Glutaminase-Dependent Metabolism. Cell 175, 1780–1795.e19. 10.1016/j.cell.2018.10.001. [PubMed: 30392958]
15. Ruvolo PP (2016). The broken "Off" switch in cancer signaling: PP2A as a regulator of tumorigenesis, drug resistance, and immune surveillance. BBA Clin 6, 87–99. 10.1016/j.bbacli.2016.08.002. [PubMed: 27556014]
16. Shi Y (2009). Serine/threonine phosphatases: mechanism through structure. Cell 139, 468–484. 10.1016/j.cell.2009.10.006. [PubMed: 19879837]
17. Katsiari CG, Kyttaris VC, Juang YT, and Tsokos GC (2005). Protein phosphatase 2A is a negative regulator of IL-2 production in patients with systemic lupus erythematosus. J. Clin. Invest 115, 3193–3204. [PubMed: 16224536]
18. Sunahori K, Juang YT, Kyttaris VC, and Tsokos GC (2011). Promoter hypomethylation results in increased expression of protein phosphatase 2A in T cells from patients with systemic lupus erythematosus. J. Immunol 186, 4508–4517. 10.4049/jimmunol.1000340. [PubMed: 21346232]

19. Crispin JC, Apostolidis SA, Rosetti F, Keszei M, Wang N, Terhorst C, Mayadas TN, and Tsokos GC (2012). Cutting edge: protein phosphatase 2A confers susceptibility to autoimmune disease through an IL-17-dependent mechanism. J. Immunol 188, 3567–3571. 10.4049/jimmunol.1200143. [PubMed: 22422882]
20. Apostolidis SA, Rodríguez-Rodríguez N, Suárez-Fueyo A, Dioufa N, Ozcan E, Crispín JC, Tsokos MG, and Tsokos GC (2016). Phosphatase PP2A is requisite for the function of regulatory T cells. Nat. Immunol 17, 556–564. 10.1038/ni.3390. [PubMed: 26974206]
21. Crispin JC, Apostolidis SA, Finnell MI, and Tsokos GC (2011). Induction of PP2A Bbeta, a regulator of IL-2 deprivation-induced T-cell apoptosis, is deficient in systemic lupus erythematosus. Proc. Natl. Acad. Sci. USA 108, 12443–12448. 10.1073/pnas.1103915108. [PubMed: 21746932]
22. Pan W, Sharabi A, Ferretti A, Zhang Y, Burbano C, Yoshida N, Tsokos MG, and Tsokos GC (2020). PPP2R2D suppresses IL-2 production and Treg function. JCI Insight 5, e138215. 10.1172/jci.insight.138215. [PubMed: 32897879]
23. Pan W, Nagpal K, Suárez-Fueyo A, Ferretti A, Yoshida N, Tsokos MG, and Tsokos GC (2021). The Regulatory Subunit PPP2R2A of PP2A Enhances Th1 and Th17 Differentiation through Activation of the GEF-H1/RhoA/ROCK Signaling Pathway. J. Immunol 206, 1719–1728. 10.4049/jimmunol.2001266. [PubMed: 33762326]
24. Lautrup S, Sinclair DA, Mattson MP, and Fang EF (2019). NAD(+) in Brain Aging and Neurodegenerative Disorders. Cell Metab 30, 630–655. 10.1016/j.cmet.2019.09.001. [PubMed: 31577933]
25. Verdin E (2015). NAD^+ in aging, metabolism, and neurodegeneration. Science 350, 1208–1213. 10.1126/science.aac4854. [PubMed: 26785480]
26. Bogan KL, and Brenner C (2008). Nicotinic acid, nicotinamide, and nicotinamide riboside: a molecular evaluation of NAD+ precursor vitamins in human nutrition. Annu. Rev. Nutr 28, 115–130. 10.1146/annurev.nutr.28.061807.155443. [PubMed: 18429699]
27. Brenner C (2022). Sirtuins are Not Conserved Longevity Genes. Life Metab 1, 122–133. 10.1093/lifemeta/loac025. [PubMed: 37035412]
28. Kropotov A, Kulikova V, Nerinovski K, Yakimov A, Svetlova M, Solovjeva L, Sudnitsyna J, Migaud ME, Khodorkovskiy M, Ziegler M, and Nikiforov A (2021). Equilibrative Nucleoside Transporters Mediate the Import of Nicotinamide Riboside and Nicotinic Acid Riboside into Human Cells. Int. J. Mol. Sci 22, 1391. 10.3390/ijms22031391. [PubMed: 33573263]
29. Nikiforov A, Dölle C, Niere M, and Ziegler M (2011). Pathways and subcellular compartmentation of NAD biosynthesis in human cells: from entry of extracellular precursors to mitochondrial NAD generation. J. Biol. Chem 286, 21767–21778. 10.1074/jbc.M110.213298. [PubMed: 21504897]
30. Muthurajan UM, Hepler MRD, Hieb AR, Clark NJ, Kramer M, Yao T, and Luger K (2014). Automodification switches PARP-1 function from chromatin architectural protein to histone chaperone. Proc. Natl. Acad. Sci. USA 111, 12752–12757, 1405005111. 10.1073/pnas.1405005111. [PubMed: 25136112]
31. Willcockson MA, Healton SE, Weiss CN, Bartholdy BA, Botbol Y, Mishra LN, Sidhwani DS, Wilson TJ, Pinto HB, Maron MI, et al. (2021). H1 histones control the epigenetic landscape by local chromatin compaction. Nature 589, 293–298. 10.1038/s41586-020-3032-z. [PubMed: 33299182]
32. Fyodorov DV, Zhou BR, Skoultchi AI, and Bai Y (2018). Emerging roles of linker histones in regulating chromatin structure and function. Nat. Rev. Mol. Cell Biol 19, 192–206. 10.1038/nrm.2017.94. [PubMed: 29018282]
33. Lai S, Jia J, Cao X, Zhou PK, and Gao S (2021). Molecular and Cellular Functions of the Linker Histone H1.2. Front. Cell Dev. Biol 9, 773195. 10.3389/fcell.2021.773195. [PubMed: 35087830]
34. Zheng Y, Josefowicz S, Chaudhry A, Peng XP, Forbush K, and Rudensky AY (2010). Role of conserved non-coding DNA elements in the Foxp3 gene in regulatory T-cell fate. Nature 463, 808–812. 10.1038/nature08750. [PubMed: 20072126]
35. Wang X, Zhang Y, Yang XO, Nurieva RI, Chang SH, Ojeda SS, Kang HS, Schluns KS, Gui J, Jetten AM, and Dong C (2012). Transcription of Il17 and Il17f is controlled by conserved noncoding sequence 2. Immunity 36, 23–31. 10.1016/j.immuni.2011.10.019. [PubMed: 22244845]

36. Cerboni B, Morozzi G, Galeazzi M, Bellisai F, Micheli V, Pompucci G, and Sestini S (2009). Poly(ADP-ribose) polymerase activity in systemic lupus erythematosus and systemic sclerosis. Hum. Immunol 70, 487–491. 10.1016/j.humimm.2009.04.021. [PubMed: 19376176]
37. Chaitanya GV, Steven AJ, and Babu PP (2010). PARP-1 cleavage fragments: signatures of cell-death proteases in neurodegeneration. Cell Commun. Signal 8, 31. 10.1186/1478-811X-8-31. [PubMed: 21176168]
38. Kim MY, Zhang T, and Kraus WL (2005). Poly(ADP-ribosyl)ation by PARP-1: 'PAR-laying' NAD+ into a nuclear signal. Genes Dev 19, 1951–1967. 10.1101/gad.1331805. [PubMed: 16140981]
39. Crispin JC, and Tsokos GC (2010). Interleukin-17-producing T cells in lupus. Curr. Opin. Rheumatol 22, 499–503. 10.1097/BOR.0b013e32833c62b0. [PubMed: 20592603]
40. Crispin JC, and Tsokos GC (2010). IL-17 in systemic lupus erythematosus. J. Biomed. Biotechnol 2010, 943254. 10.1155/2010/943254. [PubMed: 20379379]
41. Crispin JC, and Tsokos GC (2009). Human TCR-alpha beta+ CD4- CD8- T cells can derive from CD8+ T cells and display an inflammatory effector phenotype. J. Immunol 183, 4675–4681. 10.4049/jimmunol.0901533. [PubMed: 19734235]
42. Katsuyama E, Suarez-Fueyo A, Bradley SJ, Mizui M, Marin AV, Mulki L, Krishfield S, Malavasi F, Yoon J, Sui SJH, et al. (2020). The CD38/NAD/SIRTUIN1/EZH2 Axis Mitigates Cytotoxic CD8 T Cell Function and Identifies Patients with SLE Prone to Infections. Cell Rep 30, 112–123.e4. 10.1016/j.celrep.2019.12.014. [PubMed: 31914379]
43. Buang N, Tapeng L, Gray V, Sardini A, Whilding C, Lightstone L, Cairns TD, Pickering MC, Behmoaras J, Ling GS, and Botto M (2021). Type I interferons affect the metabolic fitness of CD8(+) T cells from patients with systemic lupus erythematosus. Nat. Commun 12, 1980. 10.1038/s41467-021-22312-y. [PubMed: 33790300]
44. Chen PM, Katsuyama E, Satyam A, Li H, Rubio J, Jung S, Andrzejewski S, Becherer JD, Tsokos MG, Abdi R, and Tsokos GC (2022). CD38 reduces mitochondrial fitness and cytotoxic T cell response against viral infection in lupus patients by suppressing mitophagy. Sci. Adv 8, eabo4271. 10.1126/sciadv.abo4271. [PubMed: 35704572]
45. Bieganowski P, and Brenner C (2004). Discoveries of nicotinamide riboside as a nutrient and conserved NRK genes establish a Preiss-Handler independent route to NAD+ in fungi and humans. Cell 117, 495–502. 10.1016/s0092-8674(04)00416-7. [PubMed: 15137942]
46. Wu J, Singh K, Lin A, Meadows AM, Wu K, Shing V, Bley M, Hassanzadeh S, Huffstutler RD, Schmidt MS, et al. (2022). Boosting NAD+ blunts TLR4-induced type I IFN in control and systemic lupus erythematosus monocytes. J. Clin. Invest 132, e139828. 10.1172/JCI139828. [PubMed: 35025762]
47. Littman DR, and Rudensky AY (2010). Th17 and regulatory T cells in mediating and restraining inflammation. Cell 140, 845–858. 10.1016/j.cell.2010.02.021. [PubMed: 20303875]
48. Shin MS, Lee N, and Kang I (2011). Effector T-cell subsets in systemic lupus erythematosus: update focusing on Th17 cells. Curr. Opin. Rheumatol 23, 444–448. 10.1097/BOR.0b013e328349a255. [PubMed: 21720245]
49. Yang XO, Panopoulos AD, Nurieva R, Chang SH, Wang D, Watowich SS, and Dong C (2007). STAT3 regulates cytokine-mediated generation of inflammatory helper T cells. J. Biol. Chem 282, 9358–9363. 10.1074/jbc.C600321200. [PubMed: 17277312]
50. Ivanov II, McKenzie BS, Zhou L, Tadokoro CE, Lepelley A, Lafaille JJ, Cua DJ, and Littman DR (2006). The orphan nuclear receptor RORgammat directs the differentiation program of proinflammatory IL-17+ T helper cells. Cell 126, 1121–1133. 10.1016/j.cell.2006.07.035. [PubMed: 16990136]
51. Yao Z, Kanno Y, Kerenyi M, Stephens G, Durant L, Watford WT, Laurence A, Robinson GW, Shevach EM, Moriggl R, et al. (2007). Nonredundant roles for Stat5a/b in directly regulating Foxp3. Blood 109, 4368–4375. 10.1182/blood-2006-11-055756. [PubMed: 17227828]
52. Burchill MA, Yang J, Vogtenhuber C, Blazar BR, and Farrar MA (2007). IL-2 receptor beta-dependent STAT5 activation is required for the development of Foxp3+ regulatory T cells. J. Immunol 178, 280–290. 10.4049/jimmunol.178.1.280. [PubMed: 17182565]

53. Kim MY, Mauro S, Gévry N, Lis JT, and Kraus WL (2004). NAD+--dependent modulation of chromatin structure and transcription by nucleosome binding properties of PARP-1. Cell 119, 803–814. 10.1016/j.cell.2004.11.002. [PubMed: 15607977]

54. Trammell SAJ, Schmidt MS, Weidemann BJ, Redpath P, Jaksch F, Dellinger RW, Li Z, Abel ED, Migaud ME, and Brenner C (2016). Nicotinamide riboside is uniquely and orally bioavailable in mice and humans. Nat. Commun 7, 12948. 10.1038/ncomms12948. [PubMed: 27721479]

55. Elhassan YS, Kluckova K, Fletcher RS, Schmidt MS, Garten A, Doig CL, Cartwright DM, Oakey L, Burley CV, Jenkinson N, et al. (2019). Nicotinamide Riboside Augments the Aged Human Skeletal Muscle NAD(+) Metabolome and Induces Transcriptomic and Anti-inflammatory Signatures. Cell Rep 28, 1717–1728.e6. 10.1016/j.celrep.2019.07.043. [PubMed: 31412242]

56. Kelley VE, and Roths JB (1985). Interaction of mutant lpr gene with background strain influences renal disease. Clin. Immunol. Immunopathol 37, 220–229. 10.1016/0090-1229(85)90153-9. [PubMed: 4042431]

57. Morse HC 3rd, Roths JB, Davidson WF, Langdon WY, Fredrickson TN, and Hartley JW (1985). Abnormalities induced by the mutant gene, lpr. Patterns of disease and expression of murine leukemia viruses in SJL/J mice homozygous and heterozygous for lpr. J. Exp. Med 161, 602–616. 10.1084/jem.161.3.602. [PubMed: 2982991]

58. Yuan M, Breitkopf SB, Yang X, and Asara JM (2012). A positive/negative ion-switching, targeted mass spectrometry-based metabolomics platform for bodily fluids, cells, and fresh and fixed tissue. Nat. Protoc 7, 872–881. 10.1038/nprot.2012.024. [PubMed: 22498707]

59. Xia J, and Wishart DS (2011). Web-based inference of biological patterns, functions and pathways from metabolomic data using MetaboAnalyst. Nat. Protoc 6, 743–760. 10.1038/nprot.2011.319. [PubMed: 21637195]

60. Kikawada E, Lenda DM, and Kelley VR (2003). IL-12 deficiency in MRL-Fas(lpr) mice delays nephritis and intrarenal IFN-gamma expression, and diminishes systemic pathology. J. Immunol 170, 3915–3925. 10.4049/jimmunol.170.7.3915. [PubMed: 12646661]

61. Sisirak V, Sally B, D'Agati V, Martinez-Ortiz W, Özçakar ZB, David J, Rashidfarrokhi A, Yeste A, Panea C, Chida AS, et al. (2016). Digestion of Chromatin in Apoptotic Cell Microparticles Prevents Autoimmunity. Cell 166, 88–101. 10.1016/j.cell.2016.05.034. [PubMed: 27293190]

Highlights

- PPP2R2A deficiency in T cells attenuates autoimmunity and nephritis in lupus-prone mice
- PPP2R2A deficiency promotes NAD^+ biosynthesis through NR-directed salvage pathway
- NR inhibits Th17 and promotes Treg cell differentiation by PARylating histone H1.2
- NR inhibits lupus nephritis in mice and limits the proinflammatory cytokines of SLE T cells

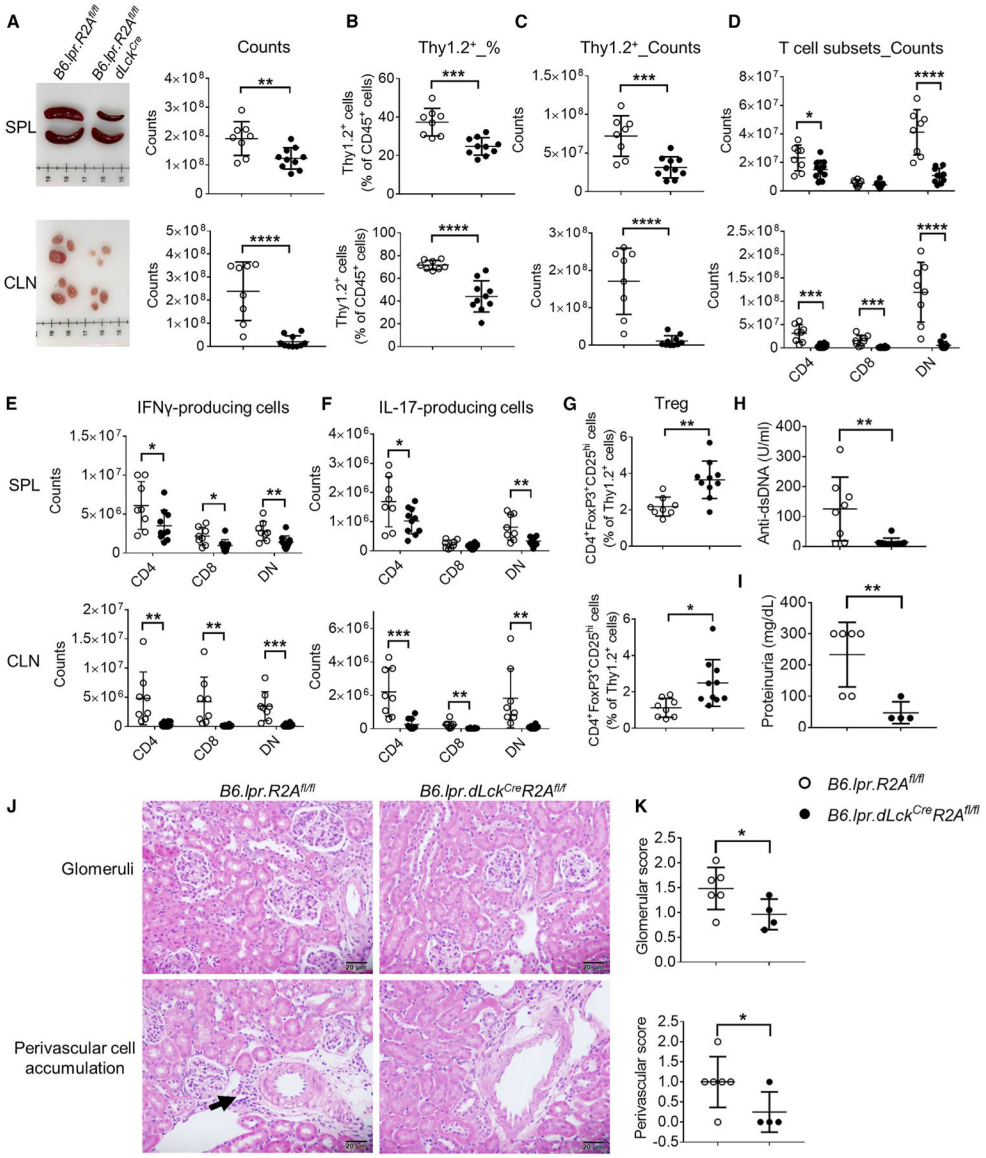

Figure 1. PPP2R2A deficiency in T cells alleviates disease in lupus-prone mice

(A–F) *B6.lpr.R2A*$^{fl/fl}$ (wild type, $n = 8$) *and B6.lpr.dLck*^{Cre}*R2A*$^{fl/fl}$ ($n = 10$) mice (26 weeks old) were euthanized for collection of SPLs and CLNs and subsequently analyzed by fluorescence-activated cell sorting (FACS). (A) Representative photographs (left) and cumulative data of the cell numbers (right) in SPLs and CLNs. Percentages (B) and numbers (C) of T cells ($CD45^+Thy1.2^+$), and numbers of CD4 ($Thy1.2^+CD4^+CD8^-$), CD8 ($Thy1.2^+CD4^-CD8^+$) and DN ($Thy1.2^+CD4^-CD8^-$) T cells (D) in SPLs and CLNs. Numbers of IFN-γ-producing ($Thy1.2^+CD4^+$IFN-γ^+, $Thy1.2^+CD8^+$IFN-γ^+, and $Thy1.2^+CD4^-CD8^-$IFN-γ^+; E) and IL-17A-producing ($Thy1.2^+CD4^+$IL-17^+, $Thy1.2^+CD8^+$IL-17^+ and $Thy1.2^+CD4^-CD8^-$IL-17^+; F) cells in SPLs and CLNs. (G) Percentage of Treg cells ($Thy1.2^+CD4^+Foxp3^+CD25^{hi}$) in SPLs and CLNs. (H–K) *B6.lpr.R2A*$^{fl/fl}$ ($n = 6$) *and B6.lpr.dLck*^{Cre}*R2A*$^{fl/fl}$ ($n = 4$) mice 35 weeks old were studied. (H) ELISA measurement of anti-dsDNA IgG levels in the serum. (I) Proteinuria by

urine strip test. (J) Representative images of kidney sections. The arrow points to a small perivascular mononuclear cell accumulation. H&E; scale bar: 20 μm. (K) Cumulative data of the histopathologic scores in the kidneys of the indicated mice. Mean ± SD is shown. *$p < 0.05$; **$p < 0.01$; ***$p < 0.001$; and ****$p < 0.0001$ using unpaired t test (A–C, G–I, and K) or multiple t test (D–F).

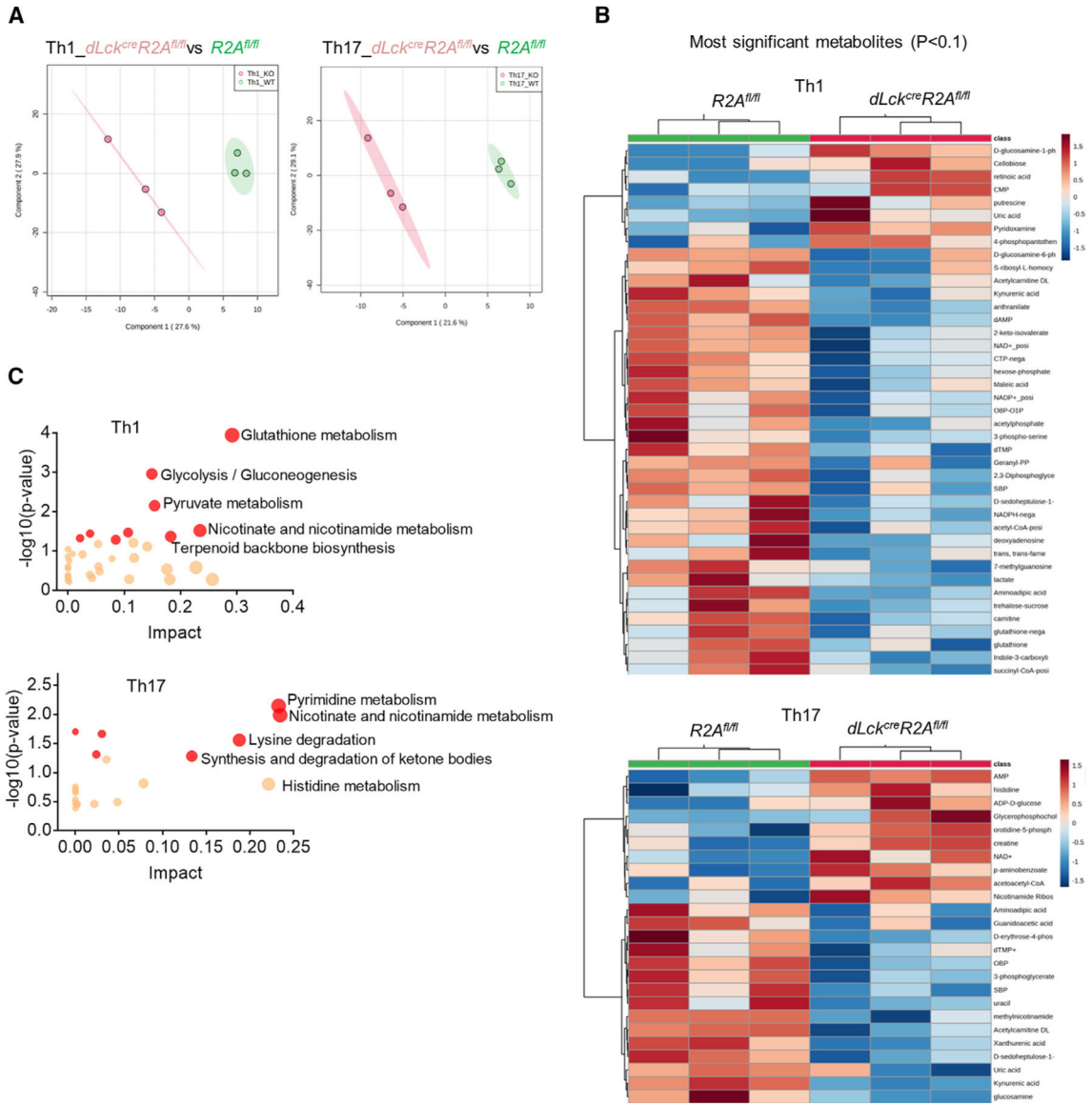

Figure 2. PPP2R2A deficiency in T cells alters metabolite profile under Th1 and Th17 polarization conditions

Metabolomics analysis was performed on PPP2R2A wild-type ($R2A^{fl/fl}$) or PPP2R2A knockout ($dLck^{Cre}R2A^{fl/fl}$) naive CD4 T cells after culture under Th1 and Th17 polarization conditions for 24 h ($n = 3$ mice/group).

(A) PCA of the metabolites of $R2A^{fl/fl}$ and $dLck^{Cre}R2A^{fl/fl}$ Th1 (left) or Th17 (right) cells.

(B) Heatmap showing the significantly ($p < 0.1$) altered metabolites in $R2A^{fl/fl}$ or $dLck^{Cre}R2A^{fl/fl}$ Th1 (up) or Th17 (down) cells.

(C) Significantly altered metabolites in PPP2R2A-deficient Th1 (up) or Th17 (down) cells were analyzed by metabolite set enrichment analysis.

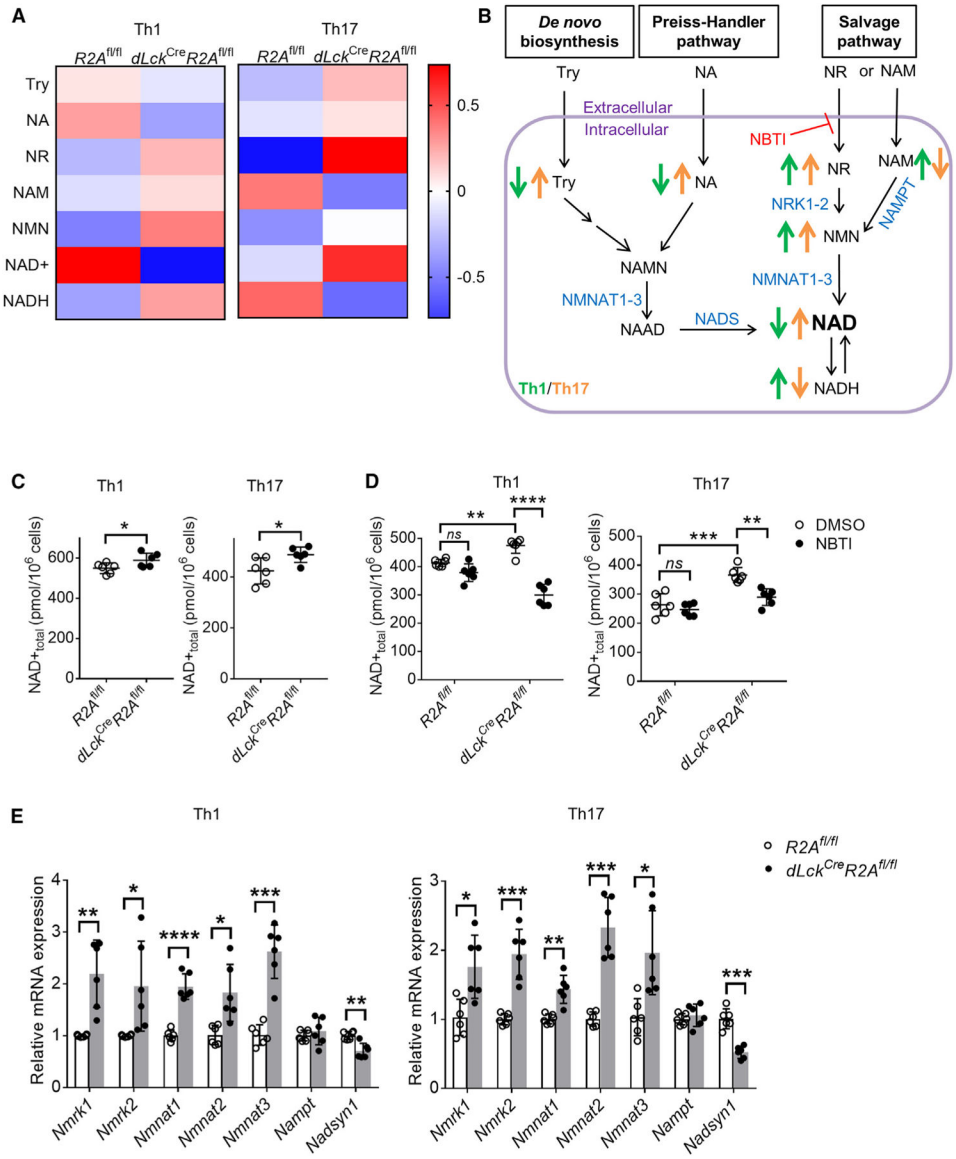

Figure 3. PPP2R2A deficiency in T cells enhances NAD+ production through the NR-directed NAD+ biosynthesis pathway

(A) Metabolomics analysis was performed on PPP2R2A wild-type (*R2A*$^{fl/fl}$) or PPP2R2A knockout (*dLck*^{Cre}*R2A*$^{fl/fl}$) naive CD4 T cells after culture under Th1 or Th17 polarization condition for 24 h (n = 3 mice/group). Relative levels of metabolites involved in the NAD$^+$ biosynthesis in *R2A*$^{fl/fl}$ and *dLck*^{Cre}*R2A*$^{fl/fl}$ Th1 or Th17 cells.

(B) Summary of the changes of metabolites in 3 NAD$^+$ biosynthesis pathways in PPP2R2A-deficient Th1 or Th17 cells. The summary was based on the data from (A). NAMN, nicotinic acid mononucleotide; NMNAT1–3: NAM mononucleotide adenyl-transferases 1–3; NAMPT, NAM phosphoribosyltransferase.

(C and D) Quantification of NAD$^+_{total}$ (NAD$^+$ and NADH) in *R2A*$^{fl/fl}$ and *dLck*^{Cre}*R2A*$^{fl/fl}$ naive CD4 T cells cultured under Th1 or Th17 cell differentiation conditions and in the presence of DMSO or NBTI (10 μM) for 24 h (D). Total NAD$^+$ (NAD$^+_{total}$) levels

were measured using a NAD/NADH quantification kit. The data were generated from 3 independent experiments.

(E) $R2A^{fl/fl}$ and $dLck^{Cre}R2A^{fl/fl}$ naive CD4 T cells were cultured under Th1 or Th17 cell differentiation conditions for 24 h before RNA was extracted for qPCR analysis. The data were generated from 3 independent experiments. Mean ± SD is shown.

ns, no significance; *$p < 0.05$; **$p < 0.01$; ***$p < 0.001$; and ****$p < 0.0001$ using unpaired t test.

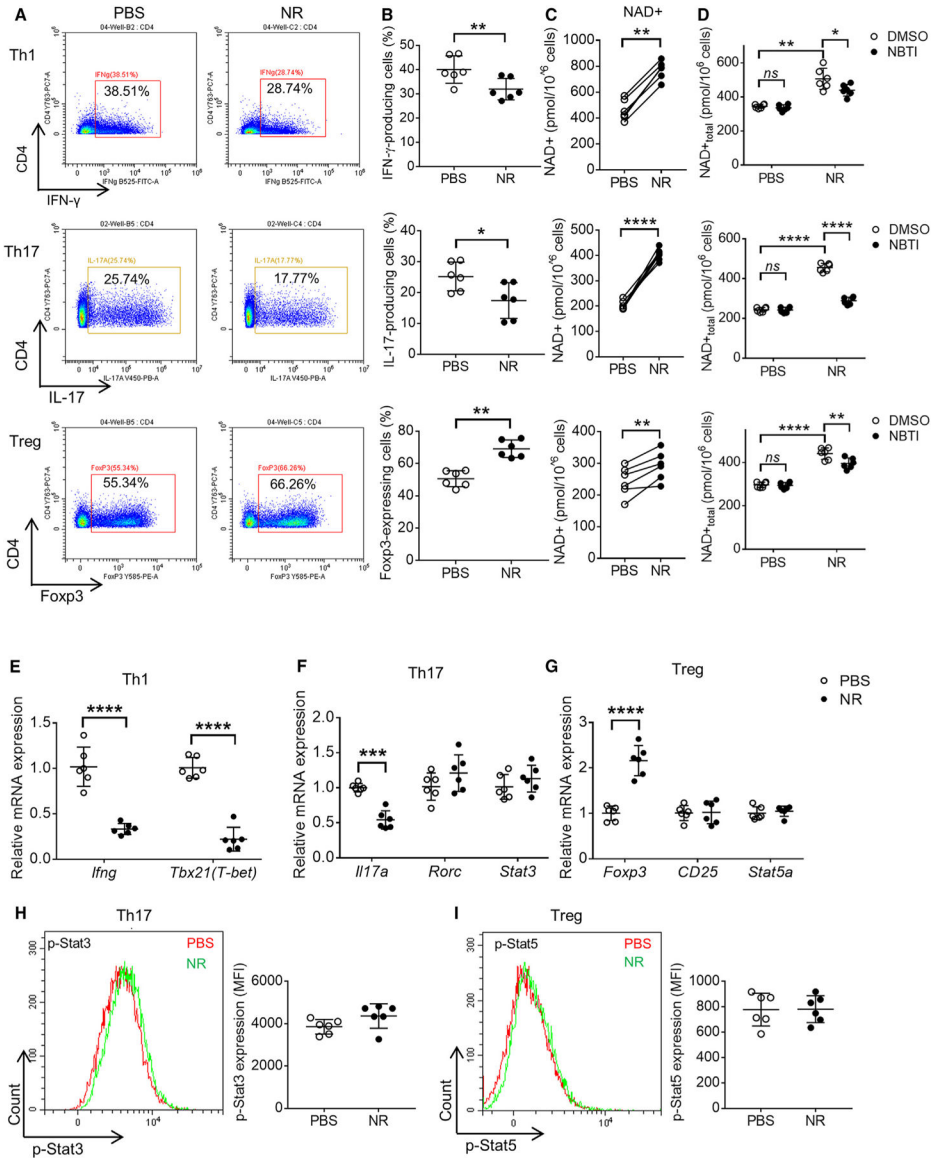

Figure 4. NR inhibits Th1 and Th17 cell differentiation but augments Treg cell differentiation in vitro

(A, B, and E–I) Naive CD4$^+$ T cells isolated from the SPLs *of R2A$^{fl/fl}$* mice were cultured under Th1-, Th17-, or Treg-polarizing conditions in the presence of PBS or NR (500 μM) for 72 h (A and B) or 24 h (C, E–I) *in vitro*.

(D) Naive CD4$^+$ T cells isolated from the SPLs *of R2A$^{fl/fl}$* mice were cultured under Th1-, Th17-, or Treg-polarizing conditions in the presence of PBS or NR (500 μM) with DMSO or NBTI (10 μM) for 24 h.

Cells were stained with the indicated antibodies before FACS analysis (A and B) or were lysed using an NAD extraction buffer (C and D). Representative flow cytometry plots are shown in (A). Cumulative data (n = 3 mice/group, duplicate) depicting the percentages of IFN-γ (Th1)- and IL-17A (Th17)-producing cells and Foxp3 (Treg)-expressing cells (B) and NAD$^+$ levels measured by ELISA kit (C and D) are shown.

(E–G) qPCR analysis of indicated gene expression. The data were generated from 3 independent experiments.

(H and I) FACS analysis of p-Stat3 or p-Stat5 expression in Th17 (H) and Treg (I) cells with PBS or NR treatment. Representative flow plots (left) and cumulative data ($n = 3$ mice/group, duplicate) of mean fluorescence intensity (right) are shown. Mean ± SD is shown. ns, no significance; *$p < 0.05$; **$p < 0.01$; ***$p < 0.001$; and ****$p < 0.0001$ using unpaired t test.

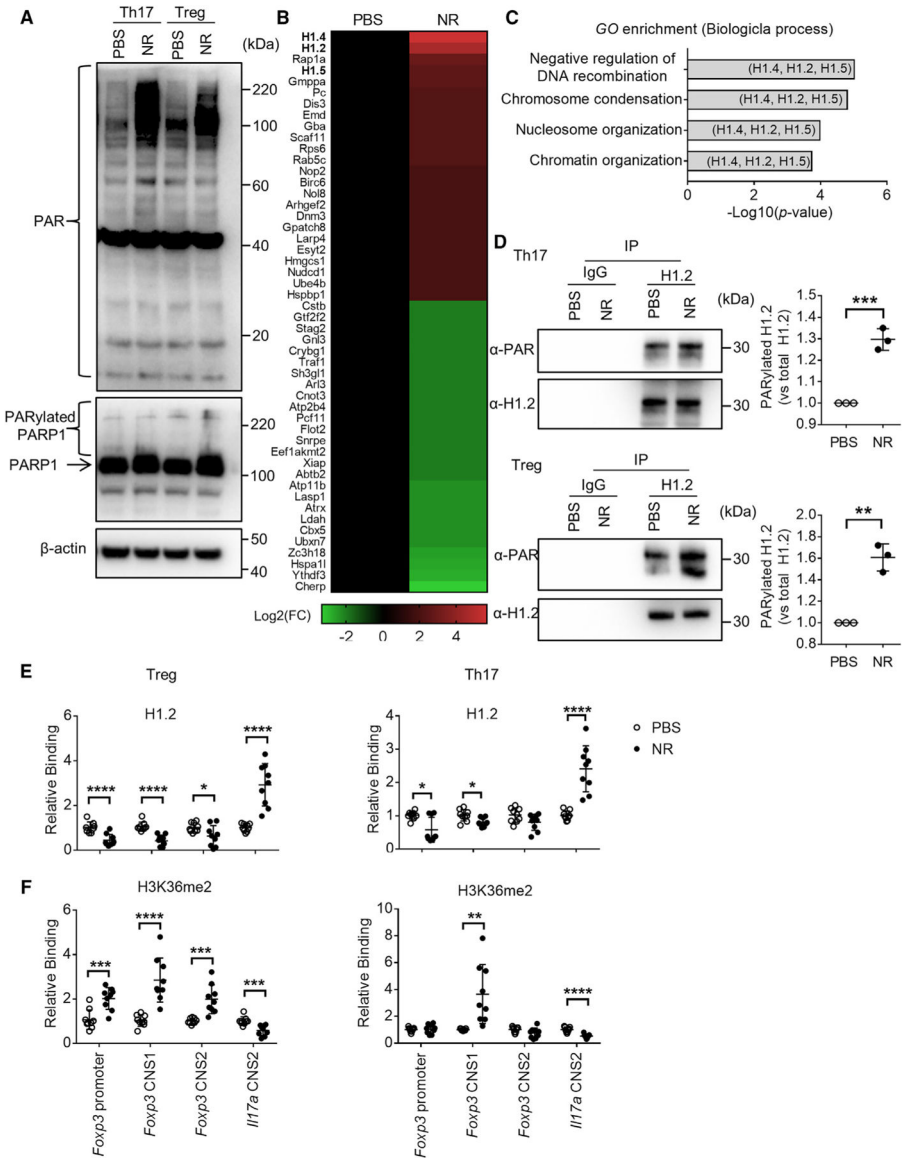

Figure 5. NR treatment alters the occupancy of histone H1 protein in Il17a and Foxp3 loci

(A) After CD4 naive T cells were cultured under Th17 and Treg cell polarization conditions in the presence or absence of NR for 24 h, protein lysates were extracted for western blot analysis.

(B) IP-MS analysis of PARylated proteins from naive CD4 T cells after culture under Treg cell differentiation conditions in the presence of PBS or NR for 24 h (n =2 mice/group). Significantly altered (|log2 fold change| > 2) PARylated proteins in NR-treated compared to PBS-treated cells are shown in the heatmap.

(C) GO pathway analysis of the PARylated proteins that were significantly altered in NR-treated cells.

(D) After Naive CD4 T cells were cultured under Th17 and Treg cell polarization conditions in the presence of PBS or NR for 24 h, protein lysates were immunoprecipitated with an antibody against H1.2 or IgG, and western blot analysis was applied using the indicated

antibodies. Representative blots (left) and cumulative densitometry data ($n = 3$, right) are shown. In quantification, PARylated H1.2 was first normalized to total H1.2 in PBS- or NR-treated group. Then, PBS-treated group was normalized to 1.

(E and F) ChIP-qPCR assays were performed for H1.2 and H3K36m2 at promoterCNS1 and CNS2 regions in the *Foxp3* gene locus and CNS2 region in the *Il17a* gene locus in CD4 naive T cells cultured under Th17 and Treg cell polarization conditions in the presence of PBS or NR for 24 h. The data are from 3 independent experiments. Mean ± SD is shown. $p < 0.05$; $^{**}p < 0.01$; $^{***}p < 0.001$; and $^{****}p < 0.0001$ using unpaired t test.

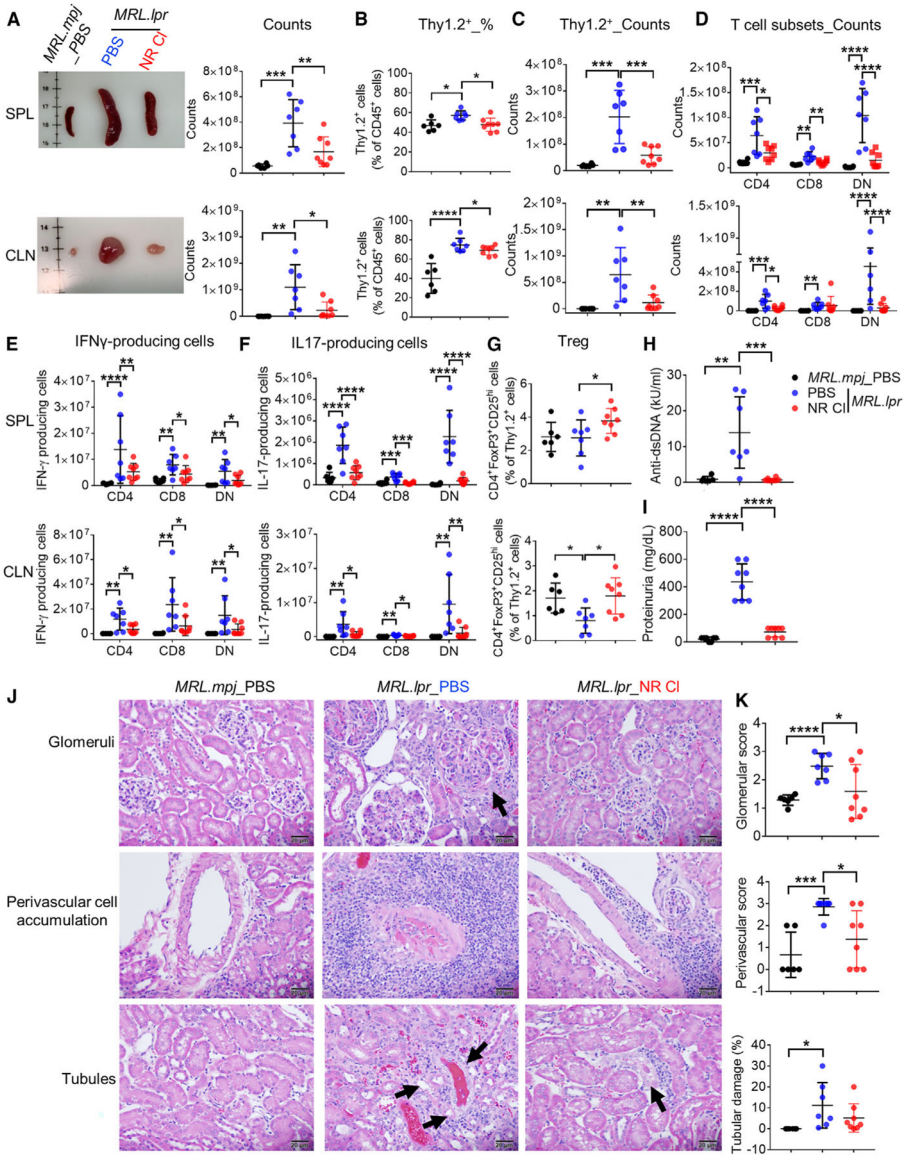

Figure 6. NR treatment alleviates lupus-related manifestations in MRL.lpr mice

To determine the role of NR in the regulation of lupus-related pathology, we intraperitoneally injected PBS (n = 7) or NR Cl (500 mg/kg body weight/day, n = 8) into 8-week-old MRL.lpr mice daily for 8 weeks. MRL.mpj (n = 6) mice injected with PBS were used as controls.

(A) The representative picture (left) and cumulative data of the cell numbers (right) of SPLs and CLNs (A).

(B–D) The percentages (B) and cell numbers (C) of T cells ($CD45^+Thy1.2^+$) and the cell numbers of CD4 ($Thy1.2^+CD4^+CD8^-$), CD8 ($Thy1.2^+CD4^-CD8^+$), and DN ($Thy1.2^+CD4^-CD8^-$) T cells (D) in SPLs and CLNs.

(E and F) The cell numbers of IFN-γ-producing ($Thy1.2^+CD4^+$IFN-γ^+, $Thy1.2^+CD8^+$IFN-γ^+, and $Thy1.2^+CD4^-CD8^-$IFN-γ^+; E) and IL-17A-producing ($Thy1.2^+CD4^+$IL-17^+, $Thy1.2^+CD8^+$IL-17^+, and $Thy1.2^+CD4^-CD8^-$IL-17^+; F) cells in SPLs and CLNs.

(G) The percentage of Treg cells (Thy1.2^{+}CD4^{+}Foxp3^{+}CD25^{hi}) in SPLs and CLNs.
(H) ELISA measurement of anti-dsDNA IgG levels in the serum.
(I) Proteinuria measured using urine strip.
(J) Representative images of glomerular, perivascular, and tubular histologic findings in kidney sections. The arrows point to a glomerular crescent (upper row) and to tubular epithelial cell vacuolization and flattening (bottom row). H&E; scale bar: 20 μm.
(K) Cumulative data of the histopathologic scores in the kidneys of mice from the indicated treatment groups. Mean ± SD is shown.
*$p < 0.05$; **$p < 0.01$; ***$p < 0.001$; and ****$p < 0.0001$ using unpaired t test (A–C, G–I, and K) or multiple *t* test (D–F).

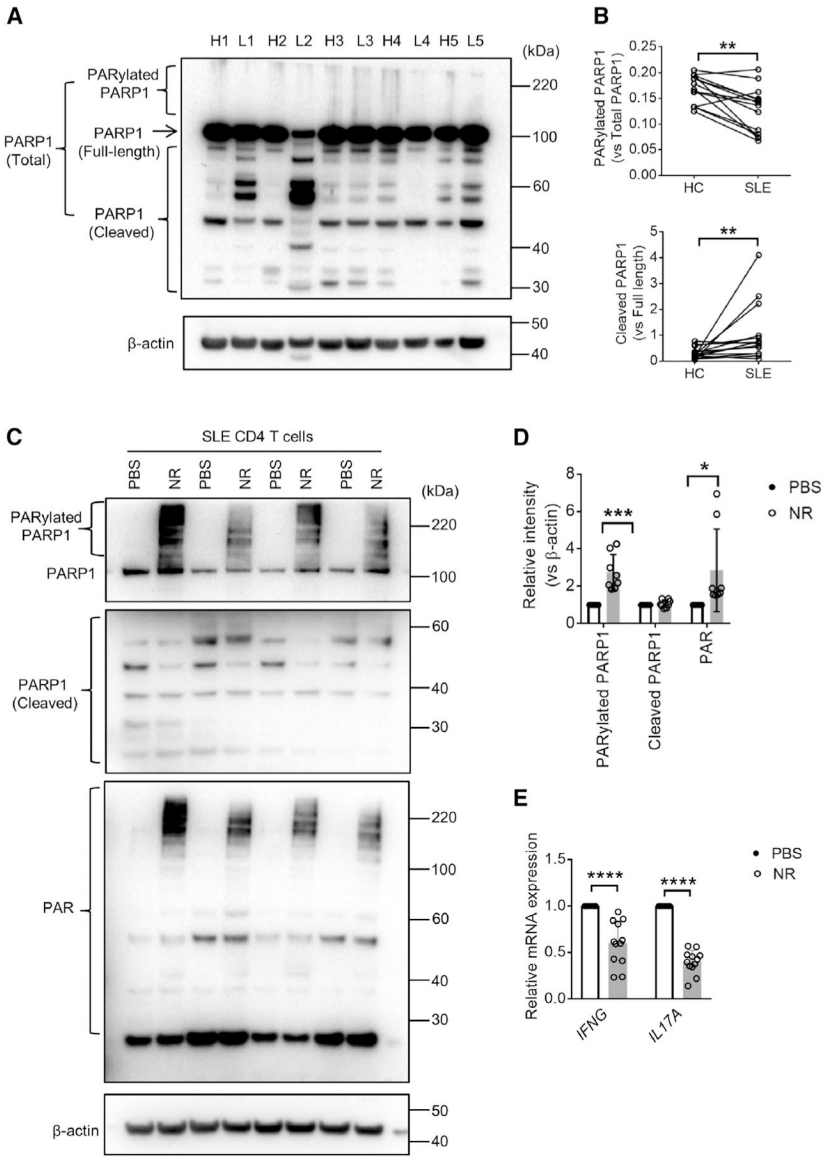

Figure 7. NR supplement restores PARP1 activity and reduces IFNG and IL17A mRNA expression in CD4 T cells from patients with SLE

(A) Western blot analysis of the protein expression levels of PARP1 and β-actin in CD4 T cells from patients with SLE or matched healthy controls. Healthy controls 1 (H1) is age, sex, and ethnicity matched with SLE patient 1 (L1); H2 is age, sex, and ethnicity matched with L2, and so on.

(B) Cumulative data for quantification of the levels of PARylated PARP1 vs. total PARP1 (top) or cleaved PARP1 vs. full-length PARP1 (bottom) in the blots shown in (A). Healthy controls (HC), $n = 14$; SLE patients, $n = 14$.

(C–E) CD4 T cells from patients with SLE were stimulated with anti-CD3/CD28 in the presence of PBS or NR for 24 h. Then, protein lysates were extracted for western blot analysis (C and D), and total RNA was isolated for qPCR analysis (E). Representative blots (C) and cumulative densitometry data ($n = 8$, D) are shown. $n = 12$ in €. Mean ± SD is shown.

**$p < 0.01$ and ****$p < 0.0001$ using paired t test (B) or multiple t test (D and E).

Table 1.

Demographic and clinical characteristics of the patients with SLE and healthy control subjects

	SLE patients (24)	Healthy controls (14)
Age, y, mean (range)	32.7 (8–59)	20.8 (8–51)
Sex, no. (%)		
Female	24 (100)	14 (100)
Male	0	0
Ethnicity, no. (%)		
White	12 (57.9)	8 (57.1)
African American	5 (26.3)	4 (28.6)
Asian	4 (15.8)	1 (7.1)
Hispanic	3 (13.3)	1 (7.1)
SLEDAI[1], mean (range)	3.67 (0–14)	–

[1]SLEDAI: Systemic lupus erythematosus disease activity index.

KEY RESOURCES TABLE

REAGENT or RESOURCE	SOURCE	IDENTIFIER
Antibodies		
Antibodies used for flow cytometry are listed in Table S2	N/A	N/A
Rabbit antibody against PARP1	Santa Cruz Biotechnology	sc-7150; RRID:AB_2160738
Mouse antibody against PAR	R&D Systems	4335-MC-100; RRID:AB_2572318
Mouse antibody against β-actin	Sigma-Aldrich	A5316; RRID:AB_476743
Mouse antibody against PPP2R2A (2G9)	Cell Signaling Technology	#5689; RRID:AB_10827877
Rabbit antibody against H1.2 (JU43-48)	Novus Biologicals	NBP2-75932; RRID:AB_2810088
Rabbit antibody against H3K36m2	Millipore-Sigma	07-274; RRID:AB_310484
Rabbit IgG control	Thermofisher Scientific	49-2024; RRID:AB_2148077
Goat anti-rabbit IgG (H + L) secondary antibody, HRP	Thermo Fisher Scientific	Cat # 31460; RRID:AB_228341
Goat anti-Mouse IgG (H + L) Secondary Antibody, HRP	Thermo Fisher Scientific	Cat # 31430; RRID:AB_228307
anti-CD3	BioLegend	145-2C11; RRID:AB_2616673
anti-CD28	BioLegend	Clone 37.51; RRID:AB_2810333
anti–IL-4	BioLegend	QA19A66; RRID:AB_2910503
anti–IFN-γ	BioLegend	XMG1.2; RRID:AB_2295769
Biological samples		
Peripheral venous blood obtained from healthy volunteers as well as patients with SLE	This study	N/A
Chemicals, peptides, and recombinant proteins		
Western ECL substrate	Bio-Rad	1705061
Nicotinamide riboside chloride	ChromaDex	TruNiagen
Nicotinamide riboside	Combi-Blocks	HB-5832
IL-12	R&D Systems	419-ML-010
TGF-β1	R&D Systems	7666-MB-005
IL-2	R&D Systems	402-ML-020
IL-6	R&D Systems	406-ML-005
Critical commercial assays		
Mouse $CD4^+CD62L$ + T cell Isolation Kit.	Miltenyi Biotec	130-104-453
NAD/NADH Quantitation Kit	Sigma-Aldrich	MAK037
MAGnify Chromatin Immunoprecipitation System	Life Technologies	49-2024
RosetteSep™ Human $CD4^+$ T cell Enrichment Cocktail	StemCell Technologies	#15022
RNeasy Plus Mini kit	QIAGEN	Cat# 74134
Dynabeads Protein G Immunoprecipitation Kit	Thermo Fisher Scientific	10007D
Experimental models: Organisms/strains		
B6.*lpr.Lck*^{Cre}*R2A*$^{fl/fl}$ mice.	This paper	N/A
B6.*lpr.R2A*$^{fl/fl}$ mice	This paper	N/A

REAGENT or RESOURCE	SOURCE	IDENTIFIER
B6.*Lck*^{Cre}*R2A*$^{fl/fl}$ mice	This paper	N/A
B6.*R2A*$^{fl/fl}$ mice	This paper	N/A
MRL.*lpr* mice	The Jackson Laboratory	Stock No: 000485
MRL.*mpj* mice	The Jackson Laboratory	Stock No: 000485
B6.*lpr* mice	The Jackson Laboratory	Stock No: 000482
Oligonucleotides		
qPCR primers are in Table S1	N/A	N/A
Software and algorithms		
Prism 7	Graphpad	Version 7.0; RRID:SCR_002798
MetaboAnalyst 5.0	Online Platform	https://www.metaboanalyst.ca/; RRID:SCR_015539
Image Lab (ChemiDoc XRS+ System)	Bio-Rad	Version 5.2.1; RRID:SCR_014210
CytExpert version 2.0	Beckman Coulter	Version 2.0; RRID:SCR_017217
FlowJo	FlowJo	Version 10.0; RRID:SCR_008520